INTEGRATED OPTICS

INTERDIGITATED - ELECTRODE SWITCHES

FINAL REPORT

Thomas K. Gaylord

December 31, 1989

U. S. ARMY RESEARCH OFFICE

Grant Number: DAAL03 - 86 - G - 0051

Georgia Institute of Technology

UNCLASSIFIED
SECURITY CLASSIFICATION OF THIS PAGE

REPORT DOCUMENTATION PAGE

1a. REPORT SECURITY CLASSIFICATION: Unclassified	1b. RESTRICTIVE MARKINGS
2a. SECURITY CLASSIFICATION AUTHORITY	3. DISTRIBUTION/AVAILABILITY OF REPORT: Approved for public release; distribution unlimited.
2b. DECLASSIFICATION/DOWNGRADING SCHEDULE	
4. PERFORMING ORGANIZATION REPORT NUMBER(S)	5. MONITORING ORGANIZATION REPORT NUMBER(S): ARO 23787.1-EL-F
6a. NAME OF PERFORMING ORGANIZATION: School of Electrical Engr. Georgia Institute of Technology; 6b. OFFICE SYMBOL (If applicable)	7a. NAME OF MONITORING ORGANIZATION: U. S. Army Research Office
6c. ADDRESS (City, State, and ZIP Code): Atlanta, Georgia 30332-0250	7b. ADDRESS (City, State, and ZIP Code): P. O. Box 12211 Research Triangle Park, NC 27709-2211
8a. NAME OF FUNDING/SPONSORING ORGANIZATION: U. S. Army Research Office; 8b. OFFICE SYMBOL (If applicable)	9. PROCUREMENT INSTRUMENT IDENTIFICATION NUMBER: DAAL03-86-G-0051
8c. ADDRESS (City, State, and ZIP Code): P. O. Box 12211 Research Triangle Park, NC 27709-2211	10. SOURCE OF FUNDING NUMBERS: PROGRAM ELEMENT NO. / PROJECT NO. / TASK NO. / WORK UNIT ACCESSION NO

11. TITLE (Include Security Classification): Integrated Optics Interdigitated-Electrode Switches

12 PERSONAL AUTHOR(S): Thomas K. Gaylord

13a. TYPE OF REPORT	13b. TIME COVERED	14. DATE OF REPORT (Year, Month, Day)	15. PAGE COUNT
Final	FROM 6-86 TO 1-90	1989 December 31	75

16. SUPPLEMENTARY NOTATION: The view, opinions and/or findings contained in this report are those of the author(s) and should not be construed as an official Department of the Army position, policy, or decision, unless so designated by other documentation.

17. COSATI CODES		
FIELD	GROUP	SUB-GROUP

18. SUBJECT TERMS (Continue on reverse if necessary and identify by block number): integrated optics, grating diffraction, switches

19 ABSTRACT (Continue on reverse if necessary and identify by block number)

The diffraction of a pure guided mode in a uniaxial anisotropic slab waveguide by a phase grating which is induced by a voltage applied to interdigitated electrodes over the waveguide has been analyzed. A pure guided mode is decomposed into four plane wave components (two ordinary and two extraordinary), which are not phase matched on the boundary between the waveguide and the grating. Thus the diffraction of a pure guided mode may be decomposed into the diffraction of four plane waves. Three-dimensional vector rigorous coupled-wave diffraction analysis of anisotropic gratings with anisotropic external regions has been used to treat the diffraction of

20. DISTRIBUTION/AVAILABILITY OF ABSTRACT: ☐ UNCLASSIFIED/UNLIMITED ☐ SAME AS RPT. ☐ DTIC USERS	21. ABSTRACT SECURITY CLASSIFICATION: Unclassified
22a. NAME OF RESPONSIBLE INDIVIDUAL	22b. TELEPHONE (Include Area Code) / 22c. OFFICE SYMBOL

DD FORM 1473, 84 MAR — 83 APR edition may be used until exhausted. All other editions are obsolete.

SECURITY CLASSIFICATION OF THIS PAGE
UNCLASSIFIED

19. Abstract (continued)

each plane wave component of the pure guided mode. Geometrical and phase/amplitude requirements are identified for the diffracted waves to constitute a guided mode. Diffracted mode efficiencies and Bragg conditions are calculated. Optic axis orientations for efficient diffraction are identified. Example calculations are presented for lithium niobate waveuide Givens rotation devices, and herringbone multiplier structures including a favorable comparison with experimental results.

I. Introduction

The diffraction of guided optical waves is of major importance in integrated optics owing to the versatility and the wide use of integrated periodic structures. Periodic interdigitated-electrode devices are widely used in integrated optics to induce phase gratings. These phase gratings can diffract guided modes and thus can function as switches[1-6], modulators,[7,8] deflectors,[5] mode converters,[9-12] strain wave transducers,[13] and perform numerical operations for optical signal processing[14-18] and optical computing[19-24] applications.

Various methods of analyzing the guided-wave diffraction have been used. The most extensively used method of analysis is the coupled-mode approach first introduced by Marcuse[25] and Kogelnik[26] and then applied to waveguide gratings.[27-41] Other methods used are the Floquet-Bloch approach,[42-44] which computes the exact modes in the perturbed region, the Green's function method,[45-47] first-order perturbation theory applied to the total field,[48-52] and the Rouard's method.[53,54] In almost all published analyses mentioned above, the interaction of the optical field with the grating is collinear which means that the incident wavevector and the grating vector are codirectional or contradirectional. Most of these analyses apply to distributed feedback lasers, distributed Bragg reflector lasers, grating couplers, filters, multiplexers and demultiplexers, deflectors, mode converters, etc. The analyses of Refs. 33, 35, 51, 53, and 54 can also treat oblique incidence on pure reflection gratings whose grating vectors are perpendicular to the boundary between the waveguide and the grating. As a result, only one transmitted and one reflected beam are possible. In Ref. 36 an approximate ray technique and an approximate coupled-beam technique (taking advantage of the paraxial beams) are used to treat grating vectors of general orientation with respect to the incident wavevector. However, only the Bragg diffracted beam is considered in that analysis. Similarly in Refs. 47 and 48 the general non-collinear case is approximately treated by retaining only the Bragg diffracted beam, using Green's functions or first-order perturbation theory respectively. Kenan[30] has ana-

lyzed approximately a more general case with many diffracted orders and modes for both polarizations using a coupled-mode/coupled-wave approach. In all the above analyses the anisotropy is completely ignored. Even though the coupled-mode theory has been extended to anisotropic media,[55] its application to non-collinear interactions is cumbersome due to the difficulties in the computation of the coupling coefficients, and in the computation of normal modes of anisotropic waveguides. As a result, very little work has been done on anisotropic guided-wave diffraction, and that which has been done is only for the case of collinear interaction.[56] However, anisotropic materials like lithium niobate are widely used in integrated optics and consequently the anisotropic properties should not be ignored.

In this paper, a new method of analyzing the diffraction of the pure guided modes of anisotropic waveguides by interdigitated-electrode induced phase gratings is presented. The analysis includes: (1) the anisotropic properties of the waveguide and of the grating, (2) the grating vector not being parallel or antiparallel with the incident mode (non-collinear diffraction problem), (3) an arbitrary number of diffracted orders retained in the analysis, (4) the conditions for mode propagation, (5) the conditions for efficient mode diffraction based on the various Bragg conditions of the plane wave components of the mode, (6) computation of the mode diffraction efficiencies, and (7) generalization of (1) through (6) for the treatment of the guided-wave diffraction by a cascaded stack of anisotropic gratings induced by interdigitated-electrodes. The analysis method described in Ref. 57 is applied for the computation of the characteristics of the induced grating. The diffraction analysis is an extension of the rigorous coupled-wave approach[58] based on the fact that a pure guided mode in an anisotropic waveguide can be decomposed into four homogeneous plane wave components (two ordinary and/or two extraordinary) that are not phase-matched at the grating boundary and consequently the diffraction problem can be decomposed into four diffraction subproblems. The analysis is restricted to uniaxial waveguides with one principal dielectric axis perpendicular to the electrode surface, and to electrode periodicities chosen such that negligible intermodal coupling occurs (or equiv-

alently for single-mode waveguides). The general approach of Ref. 59 has been adopted and modified in order to compute the effective mode indices and the fields in the film region of the waveguide for the two optic axis orientation cases. In addition, a new real transcendental equation for the computation of the mode propagation constants has been derived for the case in which the optic axis lies in the electrode plane. The conditions for mode propagation are discussed. Those are classified into geometrical conditions and amplitude and phase matching conditions. The diffracted mode parameters and efficiencies are also calculated. The analysis is generalized for slanted and cascaded electrode configurations. It has been found that the most efficient configuration occurs when the optic axis is perpendicular to the electrode surface. For the case of the optic axis lying in the electrode plane, the optic axis orientations parallel or perpendicular to the grating vector are treated. Finally, some example devices are analyzed. These include a Givens rotation device, a herringbone grating multiplier, and a hybrid mode diffraction example. In addition, a comparison with experimental data is included and an efficient configuration is suggested.

The geometry of the problem is shown in Fig. 1a. In Fig. 1b a top-view of the same configuration is shown. In both figures $(x,\ y,\ z)$ is the coordinate axis system that corresponds to the three-dimensional structure, while $(x_w,\ y_w,\ z_w)$ is the coordinate axis system of the slab uniaxial anisotropic waveguide which is rotated by an angle δ about the z axis of the $(x,\ y,\ z)$ coordinate system. The analysis is based on the given conditions: (1) The optic axis is restricted to lie in the electrode plane or perpendicular to that plane. (2) The intermodal coupling is negligible. This is automatically true if these are single-mode waveguides. (3) The evanescent-field diffraction has the same characteristics as the corresponding homogeneous plane wave diffraction. (4) The fringing effects at the grating boundaries are neglected.

II. Guided-Waves in Uniaxial Anisotropic Slab Waveguides

The modes that can propagate in uniaxial anisotropic dielectric slab waveguides are discussed in this section. The optic axis orientations in the film and the substrate regions are the same, and are restricted by the condition (1) given above. The cover is taken to be isotropic (corresponds to the buffer layer that is used for integrated electro-optic applications and it usually consists of silicon dioxide). The geometry of the waveguiding system is also shown in Fig. 1a.

The tensor relative permittivities of the film and the substrate are $\bar{\varepsilon}_f$, and $\bar{\varepsilon}_s$ respectively (expressed in the $(x_w,\ y_w,\ z_w)$ coordinate axis system), while the scalar relative permittivity of the cover is ε_c. The thickness of the waveguide (film thickness) is d and the coordinate axis system $(x_w,\ y_w,\ z_w)$ is related to the $(x,\ y,\ z)$ coordinate system by a simple translation and rotation transformation. Plane wave solutions of the form $\exp[-jk_0(k_{xwi}x_w + \beta' z_w)]$ are used where $i = c, f, s$ correspond to the cover, film, and substrate regions, respectively. The k_{xwi} and β' are the normalized wavevector components (β' is usually known as the normalized propagation constant or effective index) and $k_0 = 2\pi/\lambda_0$ where λ_0 is the freespace wavelength. Using the analysis of Refs. 59 and 60 the complex tangential electric and magnetic field components, E_{ywi}, E_{zwi}, H_{ywi}, and H_{zwi} can be written in the form

$$\frac{d\tilde{E}_i}{dx_w} = -j\tilde{A}_i\tilde{E}_i, \tag{1}$$

where $\tilde{E}_i = [E_{ywi},\ \eta_0 H_{zwi},\ E_{zwi},\ \eta_0 H_{ywi}]^T$ is a 4×1 matrix (vector), $\tilde{A}_i$ is a 4×4 matrix given in Appendix A, $i = c, f, s$, and $\eta_0 = (\mu_0/\epsilon_0)^{1/2}$, is the characteristic impedance of freespace, where ϵ_0, and μ_0 are the permittivity and the permeability of the freespace. The solution of Eq. (1) is

$$\tilde{E}_i = [\tilde{W}_i \exp(-jk_0\tilde{\Lambda}_i x_w)][\tilde{C}_i \exp(-jk_0\beta' z_w)], \tag{2}$$

where $\tilde{W}_i$ is a 4×4 matrix containing the eigenvectors of matrix $\tilde{A}_i$, $\tilde{\Lambda}_i$ is a diagonal 4×4 matrix containing the eigenvalues of $\tilde{A}_i$, and $\tilde{C}_i$ is a 4×1 matrix containing the unknown constants of the first-order differential equations [Eq. (1)]. The elements ε_{pqwi}

($p, q = x, y, z$ and $i = c, f, s$) correspond to the permittivity elements of each region and are expressed in the (x_w, y_w, z_w) coordinate axis system. The dispersion equation for the normalized propagation constant β' can be found using the boundary conditions of the problem. These are described in Appendix A. It is straightforward to show (using the expressions of Appendix A) that for nonzero solutions of the tangential fields, the normalized propagation constant β' must satisfied the equation

$$p_{33}(\beta')p_{44}(\beta') - p_{34}(\beta')p_{43}(\beta') = 0, \tag{3}$$

where $p_{ij}(\beta')$ is the ij-th element of $\tilde{P}(\beta')$, which is defined in Apppendix A. In addition, for evanescent plane wave solutions in the cover and substrate regions, and homogeneous plane wave solutions in the film region, the normalized propagation constant β' should satisfy the following inequalities

$$\beta'^2 > max\{n_{Oc}^2,\ n_{Os}^2,\ \frac{n_{Oc}^2 n_{Es}^2 \varepsilon_{zzws}}{\varepsilon_{zzws}\varepsilon_{zzws} - \varepsilon_{zzws}^2}\} \tag{4}$$

$$\beta'^2 < min\{n_{Of}^2,\ \frac{n_{Of}^2 n_{Ef}^2 \varepsilon_{zzwf}}{\varepsilon_{zzwf}\varepsilon_{zzwf} - \varepsilon_{zzwf}^2}\} \tag{5}$$

where n_{Oc}, n_{Of}, n_{Os} are the ordinary refractive indices of the cover, the film, and the substrate respectively, and n_{Ef}, n_{Es} are the principal extraordinary indices of the film and the substrate respectively. Inequality (4) guarantees that the plane waves in the cover and the substrate regions are evanescent (both ordinary and extraordinary plane waves) and inequality (5) guarantees that both ordinary and extraordinary plane waves in the film are homogeneous. Inequalities (4) and (5) satisfy also the power flow condition since no power should escape normally from the film-substrate and film-cover interfaces. The power flow condition for the two optic axis orientation cases that are considered in this chapter, are satisfied because the Poynting vector components normal to the interfaces and the corresponding wavevector components always have the same sign. That is, $S_{zwi} > 0 \Longleftrightarrow k_{zwi} > 0$ and $S_{zwi} < 0 \Longleftrightarrow k_{zwi} < 0$, for $i = c, f, s$ (S_{zwi} is the component of the Poynting vector normal to the interface). This condition is important since the power flow

in the cover and substrate regions should be zero normal to the interfaces for guidance of the light.

If inequalities (4) and (5) are satisfied then all plane wave components in the film region are homogeneous. These homogeneous plane waves for which β satisfies Eq. (3) constitute, along with the corresponding fields in the cover and the substrate, a subset of the possible guided modes in the uniaxial anisotropic waveguide.[59, 60] In this analysis, *only* these kinds of guided modes are considered. This restriction limits the angle of incidence δ when the optic axis lies in the electrode plane. Consequently, (assuming a negative birefringent material) the following inequality should hold

$$n_{Os}^2 < \frac{n_{Of}^2 n_{Ef}^2 \varepsilon_{zzwf}(\delta)}{\varepsilon_{zzwf}(\delta)\varepsilon_{xxwf}(\delta) - \varepsilon_{xzwf}^2(\delta)}, \tag{6}$$

where all the permittivity elements are expressed in the waveguide system (x_w, y_w, z_w) and consequently depend on the angle of incidence δ. In the case of positive birefringent materials the inequality for the angle of incidence δ is included in the following inequality

$$n_{Of}^2 < \frac{n_{Os}^2 n_{Es}^2 \varepsilon_{zzws}(\delta)}{\varepsilon_{zzws}(\delta)\varepsilon_{xxws}(\delta) - \varepsilon_{xzws}^2(\delta)}, \tag{7}$$

where in both cases it is assumed that the substrate ordinary and principal extraordinary refractives indices are greater than n_{Oc}. In the following subsections the two optic axis orientations under consideration are treated separately.

A. Optic Axis Perpendicular to the Electrode Surface

In this case the optic axis is oriented along the z axis (Fig. 1a). The modes are decoupled since the ordinary and the extraordinary waves can be analyzed separately. Consequently, TE and TM modes can be distinguished. Equation (3) becomes $p_{33}(\beta')p_{44}(\beta') = 0$. The condition $p_{33}(\beta) = 0$ corresponds to the guidance condition for the TE modes and is given by $2k_0 k_{xwfO} d - 2\phi_{fcO} - 2\phi_{fsO} = 2m\pi$, where

$k_{xf0} = (n_{0f}^2 - \beta'^2)^{1/2}$, $\phi_{fc0} = \tan^{-1}\{|k_{xc}|/k_{xf0}\}$, $\phi_{f,0} = \tan^{-1}\{|k_{x,0}|/k_{xf0}\}$, $k_{xc} = -j(\beta'^2 - n_{0c}^2)^{1/2}$, and $k_{x,0} = -j(\beta'^2 - n_{0,}^2)^{1/2}$. The integer m takes the values 0, 1, 2,..., and is characteristic of the TE_m mode. The field expressions can be found using Eq. (2). In this work only the expressions for the fields in the film region are going to be presented since only these are needed in the remaining analysis. Those expressions are given in Appendix A [Eqs. (A5)-(A8)].

Due to the guidance condition, Eq. (3), one parameter of the problem can be chosen arbitrarily (depending on the initial conditions of the problem as for example given by the input power). This parameter is chosen to be S_{0-} [Eq. (A4)]. Consequently, the coefficients F_{0+}, and F_{0-} (complex in general) are not independent, and their ratio differs for each TE mode. These coefficients can be written as $F_{0+} = A_0[\exp(-j\phi_{f,0})]S_{0-}$, $F_{0-} = A_0[\exp(+j\phi_{f,0})]S_{0-}$, where $A_0 = (1/2)(1 + |k_{x,0}|^2/k_{xf0}^2)^{1/2}$, and $\phi_{f,0}$ has been previously defined.

The condition $p_{44}(\beta') = 0$ corresponds to the guidance condition for the TM modes and is given by $2k_0 k_{xfE} d - 2\phi_{fcE} - 2\phi_{f,E} = 2m\pi$, where $k_{xfE} = (n_{0f}/n_{Ef})(n_{Ef}^2 - \beta'^2)^{1/2}$, $\phi_{fcE} = \tan^{-1}\{n_{0f}^2|k_{xc}|/n_{0c}^2 k_{xfE}\}$, $\phi_{f,E} = \tan^{-1}\{n_{0f}^2|k_{x,E}|/n_{0,}^2 k_{xfE}\}$, and $k_{x,E} = -j(n_{0,}/n_{E,})(\beta'^2 - n_{E,}^2)^{1/2}$. The integer m takes the values 0, 1, 2,..., and is characteristic of the TM_m mode. The field expressions can be found using Eq. (2). Similarly to the TE mode case the fields only in the film region are needed and are given in Appendix A [Eqs.(A9)-(A12)].

For the TM mode case the free parameter is chosen to be S_{E-} [Eq. (A4)]. Consequently, the coefficients F_{E+}, and F_{E-} (complex in general) are not independent, and their ratio differs for each TM mode. These coefficients can be written as, $F_{E+} = A_E[\exp(-j\phi_{f,E})]S_{E-}$, $F_{E-} = A_E[\exp(+j\phi_{f,E})]S_{E-}$, where $A_E = (1/2)(1 + n_{0f}^4|k_{x,E}|^2/n_{0,}^4 k_{xfE}^2)^{1/2}$, and $\phi_{f,E}$ have been previously defined.

B. Optic Axis Lying in the Plane of the Electrodes

In this subsection the optic axis lying in the xy plane is treated. The general theory of Refs. 59 and 60 is again being used. The guidance condition for the hybrid modes in this case is derived for the first time in the form of an analytical transcendental equation similar to the TE and TM modes. This condition is given in general by Eq. (3) which for this optic axis orientation becomes

$$\begin{aligned}
&G_O H_O F_{OO} F_{OE} \cos(g_O + h_O) \sin(\phi_{OE} - \phi_{OO}) + \\
&G_E H_E F_{EE} F_{EO} \cos(g_E + h_E) \sin(\phi_{EE} - \phi_{EO}) + \\
&G_O H_E F_{OO} F_{EE} [\sin(\alpha_O + \alpha_E + \phi_{OO} + \phi_{EE} + g_O - h_E) - \\
&\qquad \sin(\alpha_O - \alpha_E + \phi_{OO} - \phi_{EE} + g_O + h_E)] - \\
&G_O H_E F_{OE} F_{EO} [\sin(\alpha_O + \alpha_E + \phi_{OE} + \phi_{EO} + g_O - h_E) - \\
&\qquad \sin(\alpha_O - \alpha_E + \phi_{OE} - \phi_{EO} + g_O + h_E)] + \\
&G_E H_O F_{OE} F_{EO} [\sin(\alpha_O + \alpha_E + \phi_{EO} + \phi_{OE} + g_E - h_O) - \\
&\qquad \sin(\alpha_E - \alpha_O + \phi_{EO} - \phi_{OE} + g_E + h_O)] - \\
&G_E H_O F_{OO} F_{EE} [\sin(\alpha_O + \alpha_E + \phi_{OO} + \phi_{EE} + g_E - h_O) - \\
&\qquad \sin(\alpha_E - \alpha_O + \phi_{EE} - \phi_{OO} + g_E + h_O)] = 0
\end{aligned} \tag{8}$$

where F_{OO}, F_{OE}, F_{EO}, F_{EE}, G_O, G_E, H_O, H_E, α_O, α_E, g_O, g_E, h_O, h_E, ϕ_{OO}, ϕ_{OE}, ϕ_{EO}, and ϕ_{EE} are defined in the Appendix B. All the above parameters are functions of the normalized propagation constant, β' [which is the unknown of Eq. (8)], the ordinary and principal extraordinary refractive indices of the cover, the film and the substrate regions, the thickness of the waveguide, d, the orientation of the optic axis and the angle of incidence. The fields in the film region can be found in a similar manner to that previously presented and are given in Appendix B [Eqs. (B10)–(B15)]. Similarly to the decoupled TE and TM cases, the coefficients F_{O+}, F_{O-}, F_{E+}, and F_{E-} that appear in the field expressions are not independent. Again there is the possibility of one free

parameter, which as in the previous cases is chosen to be S_{O-}. Consequently the following expressions can be written: $F_{O+} = B_O[\exp(-j\vartheta_O)]S_{O-}$, $F_{O-} = B_O[\exp(+j\vartheta_O)]S_{O-}$, $F_{E+} = B_E[\exp(-j\vartheta_E)]S_{O-}$, $F_{E-} = B_E[\exp(+j\vartheta_E)]S_{O-}$, where B_O, B_E, ϑ_O, and ϑ_E are given in Appendix B.

III. Electro-optically Induced Phase Grating

When a voltage is applied to the interdigitated electrodes (usually a *dc* voltage or a quasi-static voltage), a phase grating is formed inside the waveguide under the electrodes. This is due to the linear electro-optic effect (Pockels effect). The induced grating is periodic along the x direction (Fig. 1a) and decays exponentially along the z direction since the inducing electric field has the same properties. Consequently, using the expressions of Ref. 57, the optical relative permittivity tensor elements in the waveguiding region (film) are

$$\varepsilon_{uv}(x,z) \simeq \varepsilon_{uv0} + \sum_{m,\ odd} A_m g_m(z)\phi_m(x), \tag{9}$$

where $u,v = x,y,z$ and ε_{uv0} is given in Ref. 57, A_m is a constant factor that depends on the electrode geometry, the material parameters, the applied voltage, and the spatial harmonic number m. The constant A_m is given in Ref. 57. In addition, $g_m(z) = \exp[-\pi m a_4(z - t - d_c)/\Lambda_e]$, where $2t$ is the electrode thickness, d_c is the buffer layer (cover) thickness, and a_4 is also defined in Ref. 57. Finally, $\phi_m(x) = \sin(\pi m x/\Lambda_e)$ where Λ_e is the electrode spacing. The above relative optical permittivity tensor elements do not vary along the $\pm y$ direction and are expressed in the (x, y, z) coordinate axis system.

In order to account for the variation along the z direction, two approaches can be used; (a) averaging of the electric field (electrostatic or quasi-static field) with respect to z coordinate, without any optical field weighting, and (b) averaging of the electric field with respect to the z coordinate using optical field weighting. The inclusion of an optical field weighting takes into account the non-uniformity of the optical field in the film region of

the waveguide. These averaging procedures define a new quantity,

$$g_m^{eq} = \int_{z_0}^{z_1} g_m(z)dz, \tag{10}$$

which is independent of z. For the case of no optical field weighting,

$$g_m^{eq} = \int_{z_0}^{z_1} g_m(z)|E_{opt}(z)|^2 dz \Big/ \int_{z_0}^{z_1} |E_{opt}(z)|^2 dz, \tag{11}$$

where $z_0 = t + d_c$, $z_1 = t + d_c + d$, d is the film thickness, and $|E_{opt}(z)|^2 = |E_{xwf}|^2 + |E_{ywf}|^2 + |E_{zwf}|^2$, is the optical field magnitude [E_{uwf}, $u = x, y, z$ are given in Eq. (A5) or Eqs. (A9) and (A10) when the optic axis is perpendicular to the electrode surface and by Eqs. (b10)–(b12) when the optic axis is in the electrode surface]. Since the optical fields are expressed in the waveguide coordinate system (x_w, y_w, z_w), a suitable coordinate axis system transformation is necessary to express all optical fields of the incident mode in the (x, y, z) coordinate axis system. Substituting Eqs. (10) or (11) into Eq. (9) the following z independent approximate expressions for the relative optical permittivity tensor elements are found;

$$\varepsilon_{uv}^{eq}(x) \simeq \varepsilon_{uv0} + \sum_{m,\ odd} A_m g_m^{eq} \phi_m(x), \tag{12}$$

where $\varepsilon_{uv}^{eq}(x)$ is the uv-th z independent element of the relative optical permittivity tensor. Knowledge of the relative optical permittivity tensor is equivalent to knowledge of the electro-optically induced phase grating under the interdigitated electrodes inside the waveguide. This relative optical permittivity tensor is necessary to carry out the diffraction analysis.

IV. Guided Mode Decomposition

Using the expression of Eqs. (A5)–(A8), or Eqs. (A9)–(A12), or Eqs. (B10)–(B15), the total incident optical electric and magnetic fields are

$$\vec{E}_{inc} = [\vec{E}_{O+} a_{O+}(z) + \vec{E}_{O-} a_{O-}(z) + \vec{E}_{E+} a_{E+}(z) + \vec{E}_{E-} a_{E-}(z)]b(x,y), \tag{13}$$

$$\vec{H}_{inc} = [\vec{H}_{O+} a_{O+}(z) + \vec{H}_{O-} a_{O-}(z) + \vec{H}_{E+} a_{E+}(z) + \vec{H}_{E-} a_{E-}(z)]b(x,y), \tag{14}$$

where $a_{q\pm}(z) = \exp(\pm jk_0 k_{zwfq} z)$, $q = O,\ E$, $b(x,y) = \exp[-jk_0\beta'(\sin\delta\ x - \cos\delta\ y)]$, and δ is the angle of incidence (Fig. 1a). The $\vec{E}_{q+}$, $\vec{E}_{q-}$, $\vec{H}_{q+}$, and $\vec{H}_{q-}$, terms ($q = O, E$), correspond to the vector complex constants of the incident field components. The components of the Eqs. (A5)-(A8), (A9)-(A12), and (B10)-(B15) have been transformed into the (x, y, z) coordinate axis system. Using Eqs. (13) and (14) a guided mode incident on the grating can be decomposed into four plane wave components, two ordinary $O+$ and $O-$, and two extraordinary $E+$, and $E-$. This situation is depicted in Fig. 2.

The four plane wave decomposition corresponds to the general hybrid mode case. This applies when the optic axis is in the plane of the electrodes (xy plane). For the decoupled cases, when the optic axis is perpendicular to the electrode surface (along z axis) only two out of the four plane waves exist and the mode is either TE or TM. For the TE decoupled mode case only the $O+$ and $O-$ plane waves exist, and consequently, $\vec{E}_{E+} = \vec{E}_{E-} = \vec{H}_{E+} = \vec{H}_{E-} = 0$. For the TM decoupled mode case only the $E+$ and the $E-$ plane waves exist and consequently $\vec{E}_{O+} = \vec{E}_{O-} = \vec{H}_{O+} = \vec{H}_{O-} = 0$. In this analysis it is required as mentioned before to have only homogeneous plane wave components in the film region. As a result, inequality (5) should hold. As described in Refs. 59 and 60 it is possible for a guided mode to consist of both homogeneous and inhomogeneous plane wave components in the film region. Thus, only a subset of the guided modes in uniaxial anisotropic waveguides, the subset that contains the modes decomposable into four homogeneous plane wave components in the film region, will be analyzed using the approach described in this section.

V. Decomposition of the Diffraction Problem into Four Subproblems

A guided mode that is composed (in the film region) of four homogeneous plane waves can be expressed by Eqs. (13) and (14), where k_{zwfO}, k_{zwfE}, and β' are real numbers. These four plane wave components are not phase matched on the boundary of the grating

(xz plane in Fig. 1a) since in general $k_{zwjO} \neq k_{zwjE}$. The incident electric and magnetic fields can be written as

$$\vec{E}_{inc} = \sum_q \vec{E}_q \exp(-jk_0 \vec{k}_q \cdot \vec{r}), \tag{15}$$

$$\vec{H}_{inc} = \sum_q \vec{H}_q \exp(-jk_0 \vec{k}_q \cdot \vec{r}), \tag{16}$$

where $q = O+,\ O-,\ E+,\ E-$, and $\vec{k}_q = \beta' \sin\delta\ \hat{x} - \beta' \cos\delta\ \hat{y} \pm k_{zwjq}\hat{z}$. The $+$ sign corresponds to the $O+$ and $E+$ waves and the $-$ sign corresponds to the $O-$ and $E-$ waves. Each component of Eqs. (15) and (16) satisfies the Maxwell's equations. Inside the grating region the total field is expanded into space-harmonic components by extending the expressions of Ref. 58. Those expressions are extended, however, for multiple incident waves. The resulting fields in the grating region are

$$\vec{E}_2 = \sum_q \sum_i [S^q_{x_i}(y)\hat{x} + S^q_{y_i}(y)\hat{y} + S^q_{z_i}(y)\hat{z}] b_i(x,y) a_q(z), \tag{17}$$

$$\vec{H}_2 = (\frac{\epsilon_0}{\mu_0})^{1/2} \sum_q \sum_i [U^q_{x_i}(y)\hat{x} + U^q_{y_i}(y)\hat{y} + U^q_{z_i}(y)\hat{z}] b_i(x,y) a_q(z), \tag{18}$$

where $q = O+,\ O-,\ E+,\ E-$, $b_i(x,y) = \exp\{-jk_0[(\beta' \sin\delta - iK_x)x - iK_y y]\}$, and i designates the i-th diffracted order corresponding to the q-th incident homogeneous plane wave, $\vec{K} = K_x\hat{x} + K_y\hat{y}$, is the grating vector, and $a_q(z)$'s have been previously defined. The $\vec{E}_2$ and $\vec{H}_2$ fields should satisfy the Maxwell's equations in the grating region. Substitution of Eqs. (17) and (18) into the Maxwell's equations leads to four independent sets of equations, one for every incident plane wave component (two sets of equations for the ordinary waves and two sets of equations for the extraordinary waves). The above decomposition of the Maxwell's equations into four independent sets of equations, is a result of the linear independence of the exponential terms $a_q(z)$.

$$\vec{E}_1 = \vec{E}_{inc} + \sum_q \sum_i \vec{R}^q_i \exp(-jk_0 \vec{k}^q_{1i} \cdot \vec{r}) + \vec{R}'^q_i \exp(-jk_0 \vec{k}'^q_{1i} \cdot \vec{r}), \tag{19}$$

$$\vec{E}_3 = \sum_q \sum_i \vec{T}^q_i \exp[-jk_0 \vec{k}^q_{3i} \cdot (\vec{r} + s\hat{y})] + \vec{T}'^q_i \exp[-jk_0 \vec{k}'^q_{3i} \cdot (\vec{r} + s\hat{y})], \tag{20}$$

where $\vec{E}_{inc}$ is given by Eq. (15), $q = O+,\ O-,\ E+,\ E-$, $\vec{R}_i^q$, $\vec{R}_i'^q$, $\vec{T}_i^q$, $\vec{T}_i'^q$, are the complex diffracted amplitudes of the i-order that correspond to the q incident plane wave, and k_{pi}^q, $k_{pi}'^q$ $(p = 1,3)$ are given by expressions similar to the ones described in Ref. 58 for each incident plane wave q. Using exactly the same procedure described in Ref. 58 for each incident plane wave component q, four independent sets of boundary conditions can straightforwardly be derived. Consequently, the three-dimensional anisotropic grating diffraction analysis of Ref. 58 can be applied repeatedly for each incident homogeneous plane wave component of the incident mode. In this analysis, the condition (3) described in section I is being used since the boundary conditions for the film-cover and film-substrate interfaces are not explicitly used inside the grating region. A similar condition was used by Marcuse[25] in the coupled-mode analysis of isotropic corrugated waveguides.

Summarizing, the grating diffraction problem of an incident guided mode in the uniaxial slab waveguide can be decomposed into four plane wave grating diffraction subproblems. Each subproblem corresponds to a plane wave component of the incident mode. The procedure described is shown in Fig. 3.

VI. Mode Propagation Conditions

A pure guided mode in a uniaxial dielectric slab waveguide can be decomposed into four homogeneous plane wave components. Thus, in general, one guided mode consists of both ordinary and extraordinary waves. Consequently, all types of diffraction described in Ref. 58 are possible. The OO, OE, EO, and EE types diffraction are due to the grating anisotropy and to the hybrid character of the incident mode. Since the forward- and backward-diffracted wavevectors satisfy different dispersion equations (ordinary or extraordinary), and the incident wavevectors are not phase matched along the z axis, the resulting diffraction angles, projected onto the xy plane, are not equal. This happens since every diffracted mode consists of four ordinary and four extraordinary plane waves not

necessarily lying in the same vertical plane. This situation is depicted in Fig. 1b for two forward-diffracted orders. The eight plane wave components result from the diffraction of each incident plane wave (mode component) into an ordinary and an extraordinary plane wave. Since the incident mode contains two ordinary and two extraordinary waves, eight plane waves result from the PQ types of diffraction where P, $Q = O$, E. Due to the multiple diffraction types there are corresponding multiple Bragg conditions.[58]

In order for the forward- and backward-diffracted modes to propagate the following conditions must be satisfied: (1) At least four of the eight plane wave components of every diffracted order should lie on the same vertical plane in order to constitute the four plane wave components of the mode (two of the plane waves should be ordinary, $O+$, $O-$, and two extraordinary, $E+$, $E-$). For the decoupled cases, when the optic axis is along the z axis, only two plane waves are necessary to satisfy the above condition (only two ordinary, $O+$, $O-$, in the case of TE modes and only two extraordinary, $E+$, $E-$, in the case of TM modes). (2) The propagation constant of a diffracted mode should be the same as the propagation constant of the incident mode along the diffraction direction that corresponds to that particular diffracted order (since in the uniaxial dielectric slab waveguides the mode parameters depend on the direction of the propagation with respect to the optic axis orientation). This condition is necessary to guarantee that the same type of mode will propagate in the uniaxial slab waveguide after the diffraction by the induced phase grating (since either the intermodal coupling is neglected or the waveguide supports only a single mode). (3) For efficient diffraction the same Bragg conditions should be satisfied by all the incident plane wave components of the mode. (4) Finally, the four plane wave components of the mode should satisfy a certain amplitude and phase condition which is characteristic of the incident mode. In the case of hybrid modes this condition will cause radiation losses since in general the ordinary and the extraordinary components of the mode will possess different diffraction characteristics.

Conditions (1), (2), and (3) restrict the direction of the optic axis with respect to

the grating vector orientation and the angle of incidence. They can be characterized as *geometrical* conditions since they involve geometrical requirements. Condition (4) can be characterized as *amplitude/phase* condition since it involves the amplitudes and the phases of the diffracted plane wave components. In the following subsection the above conditions are discussed and analyzed for the two optic axis orientations that are of interest.

A. Geometrical Conditions

A1. Optic Axis Perpendicular to the Electrode Surface

The case of the optic axis perpendicular to the electrode surface corresponds to the decoupled case where both TE and TM modes can be exist. Since the optic axis is along the z axis there is a cylindrical symmetry in the xy plane. Various planar slices through the wavevector surfaces are shown in Fig. 4. In this case only two waves (both ordinary or both extraordinary) exist for one specific mode. This is the reason for the two different propagation constants β'_{TE}, and β'_{TM} that are shown in Figs. 4c and 4d for a TE and a TM mode respectively. A degenerate case of both a TE and a TM mode having the same propagation constant is also possible but this is not a general case of interest.

It is straightforward to show, using the wavevector dispersion relations, that the normalized (with respect to k_0) y components of the diffracted wavevectors for the i-th diffracted order are

$$k_{yi}^{OO} = \pm(\beta_{TE}'^2 - k_{xi}^2)^{1/2}, \tag{21}$$

$$k_{yi}^{OE} = \pm\left[\left(\frac{n_{Ef}}{n_{Of}}\beta'_{TE}\right)^2 - k_{xi}^2\right]^{1/2}, \tag{22}$$

for a TE incident mode, and

$$k_{yi}^{EE} = \pm(\beta_{TM}'^2 - k_{xi}^2)^{1/2}, \tag{23}$$

$$k_{yi}^{EO} = \pm\left[\left(\frac{n_{Of}}{n_{Ef}}\beta'_{TM}\right)^2 - k_{xi}^2\right]^{1/2}, \tag{24}$$

where the + sign corresponds to backward- and − sign to forward-diffracted orders and $k_{z_i} = \beta' \sin\delta - iK_z$ (in this case due to the unslanted grating $K_z = K$ and $K_y = 0$). The $k_{y_i}^{pq}$ are the y components for the i-th diffracted order of a p polarization ($p = O,\ E$) incident and a q polarization ($q = O,\ E$) diffracted. Equations (21), (22) and (23), (24) hold for both $O+$, $O-$ waves and $E+$, $E-$ waves respectively. Consequently, condition (1) is satisfied since both $O+$, $O-$ or $E+$, $E-$ waves for a TE or a TM incident mode respectively lie in the same vertical plane. Using Eqs. (21)–(24) the diffracted angles of any diffracted order can be found from $\tan\delta_i^{pq} = \pm k_{z_i}/k_{y_i}^{pq}$. These angles are shown in Fig. 5 for the 0-order and the i-order forward-diffracted waves. In the case of a TE incident mode (Fig. 5a) both plane wave components in the directions δ_0^{OO} and δ_i^{OO} are ordinary and have the same propagation constant as the incident mode. In the directions characterized by the angles δ_0^{OE} and δ_i^{OE}, there are two extraordinary waves produced by the OE type diffraction. These two extraordinary waves can constitute a TM mode if $(n_{Ef}/n_{Of})\beta'_{TE}$ is a propagation constant corresponding to a TM mode. A similar situation is shown in Fig. 5b for a TM mode. The two ordinary waves along the δ_i^{EO} direction (produced by the EO type diffraction) can constitute a TE mode if $(n_{Of}/n_{Ef})\beta'_{TM}$ is a propagation constant that corresponds to a TE mode.

Due to the cylindrical symmetry in the xy plane (shown in Fig. 4b), it is straightforward to prove that the eigenvectors and the eigenvalues of matrices $\tilde{A}_i$ [Eq. (A1), $i = c,\ f,\ s$] are independent of the angle of incidence δ. The i-th diffracted mode has the same propagation constant, β'_{TE} or β'_{TM}, for TE or TM mode respectively (Figs. 4c and 4d). Thus, Eqs. (3)–(5) are satisfied for any diffracted order. Consequently, condition (2) is also satisfied.

The last of the geometrical conditions deals with the Bragg conditions. The Bragg condition for TE or TM modes can be derived from the expressions of Ref. 58. Both $O+$ and $O-$ waves satisfy the same Bragg condition. In addition, $E+$ and $E-$ share the same Bragg condition. For a TE-to-TE or a TM-to-TM mode diffraction, in the unslanted

electrode configuration, the Bragg condition is $\Lambda_q = \lambda_0 i/2\beta'_q \sin\delta$, where q = TE, TM, and λ_0 is the freespace incident wavelength. The geometrical conditions discussed in this section are extended in the next section for the case of the optic axis lying in the plane of the electrodes.

A2. Optic Axis in the Plane of the Electrode Surface

The case of the optic axis lying in the electrode plane (xy plane) corresponds to the hybrid mode case since neither TE nor TM modes can exist in this case. The plane intersections of the wavevector surfaces corresponding to that orientation of the optic axis are shown in Fig. 6.

Similarly to the previously case, it is straightforward to show that the normalized y components of the diffracted wavevectors are

$$k_{yi}^{OO} = \pm(\beta'^2 - k_{zi}^2)^{1/2}, \tag{25}$$

$$k_{yi}^{EE} = \frac{-\varepsilon_{xy}k_{zi}}{\varepsilon_{yy}} \pm \frac{[\beta'^2\varepsilon_{yy}(\varepsilon_{zz}\sin^2\delta_i^{EE} - \varepsilon_{xy}\sin 2\delta_i^{EE} + \varepsilon_{yy}\cos^2\delta_i^{EE}) - k_{zi}^2 n_{Of}^2 n_{Ef}^2]^{1/2}}{\varepsilon_{yy}}, \tag{26}$$

$$k_{yi}^{EO} = \pm[n_{Of}^2 - n_{Ef}^2 - k_{zi}^2 + \frac{\beta'^2}{n_{Of}^2}(\varepsilon_{zz}\sin^2\delta_i^{EE} - \varepsilon_{xy}\sin 2\delta_i^{EE} + \varepsilon_{yy}\cos^2\delta_i^{EE})]^{1/2}, \tag{27}$$

$$k_{yi}^{OE} = \frac{-\varepsilon_{xy}k_{zi} \pm [n_{Of}^2 n_{Ef}^2 \varepsilon_{yy} - k_{zi}^2 n_{Of}^2 n_{Ef}^2 - (n_{Of}^2 - \beta'^2)\varepsilon_{yy} n_{Of}^2]^{1/2}}{\varepsilon_{yy}}, \tag{28}$$

where again the + sign corresponds to backward- and the − sign to forward-diffracted wavevectors, and all the relative permittivities are expressed in the (x, y, z) coordinate axis system. The diffracted angles for any diffracted order can be found from the equation $\tan\delta_i^{pq} = \pm k_{zi}/k_{yi}^{pq}$. These angles are shown in Fig. 7. In the EE and EO type of diffractions the computation of the δ_i^{EE} and δ_i^{EO} requires the solution of a trigonometric equation.

In the general case there are four distinct propagation directions for one diffracted order due to the various types of diffraction. In Fig. 7a the different diffracted angles are shown for the 0-order and i-order forward-diffracted waves. The eight diffracted waves are distributed as follows: two ordinary waves $O+$, $O-$ along the direction of δ_i^{OO} produced by the OO type diffraction, two extraordinary waves, $E+$, $E-$ along the direction δ_i^{EE} produced by the EE type of diffraction, two ordinary waves $O+$, $O-$ along the direction δ_i^{EO} produced by the EO type diffraction, and two extraordinary waves, $E+$, $E-$ along the direction δ_i^{OE} produced by the OE type of diffraction. However, a situation like the one depicted in Fig. 7a does not satisfy geometrical condition (1) since for a mode all four waves, $O+$, $O-$, $E+$, and $E-$ do not lie in the same vertical plane. This problem does not appear for the 0-order forward-diffracted mode since as is shown in Fig. 7a all four waves lie in the same vertical plane. There is, however, a solution to that problem if the orientation of the optic axis is restricted to be along the x or the y coordinate axis. In this case it can be shown that

$$k_{yi}^{OO} = k_{yi}^{EE} = -\beta' \cos\delta, \tag{29}$$

In addition to the restriction in the optic axis orientation the Bragg condition should also be satisfied in order for Eq. (29) to hold. This situation is shown in Fig. 8 for the two optic axis orientations. It is important to note the symmetry of these two special optic axis orientations. The optic axis orientation is perpendicular or parallel to the grating vector.

The second geometrical condition is also needed. The normalized propagation constant along the 0-order and the Bragg-order forward-diffraction directions is the same with the normalized constant of the incident mode, β'. The condition expressed by Eq. (3) should also hold to guarantee the guidance of the mode. This condition for the incident mode can be written as

$$p_{33}(\delta,\beta')p_{44}(\delta,\beta') - p_{34}(\delta,\beta')p_{43}(\delta,\beta') = 0. \tag{30}$$

It is straightforward, but tedious, to show that the Bragg diffracted order at an angle $-\delta$, as it is shown in Fig. 8, will satisfy the condition (30) for $-\delta$ and β'. Consequently,

the Bragg-order forward-diffracted waves at the direction $\delta_i^{OO} = \delta_i^{EE} = -\delta$ satisfy the second geometrical condition. The third geometrical condition is concerned with the Bragg conditions. If the optic axis is along the x or the y direction and the Bragg condition is satisfied for the ordinary and the extraordinary waves, then all four plane wave components of the incident mode will satisfy the same Bragg condition that was given for the decoupled cases where $\beta_i' = \beta'$. This can be seen from Fig. 8 and can be found analytically using the expressions for the Bragg conditions.

The rest of the plane waves at the directions of the angles δ_i^{OE} and δ_i^{EO}, cannot constitute a mode since there are either only ordinary or only extraordinary components in their respective directions, and the modes for these directions must be hybrid modes. In addition, all the diffracted orders except the 0-order and the Bragg-order forward-diffracted modes cannot constitute a mode since they do not satisfy all the geometrical conditions. The modes that are diffracted in these directions will radiate into the substrate and the superstrate, and consequently, the guided mode will experience radiation losses during the diffraction by the interdigitated-electrode induced phase grating.

B. Amplitude and Phase Matching Conditions

The diffracted plane wave components of the four incident homogeneous plane waves (that constitute the incident mode) can be written in the form

$$\vec{E}_i^{p\pm} = (T_{xip\pm}\hat{x} + T_{yip\pm}\hat{y} + T_{zip\pm}\hat{z}) \exp[-jk_0(k_{xi}x + k_{yi}^{pp}y \mp k_{zwfp}z)], \qquad (31)$$

where $p = O$, E, and i corresponds to the i-order forward- or backward-diffracted wave. The above equation can be derived using the expressions of Ref. 58, where ordinary and extraordinary components have been distinguished and the $\exp(-jk_0 k_{yi}^{pp} s)$ factors (s is the grating thickness) have been included in the complex $T_{wip\pm}$ ($w = x, y, z$) wave amplitude components. Equation (31) includes only the plane wave components that lie in the vertical plane that make an angle $\delta_i^{OO} = \delta_i^{EE}$ with the y axis, since as was justified

previously, all four plane wave components $O+$, $O-$, $E+$, and $E-$, will lie in that plane if the geometrical conditions are satisfied. The total field at the direction of δ_i^{pp} is $\vec{E}_i = \vec{E}_i^{O+} + \vec{E}_i^{O-} + \vec{E}_i^{E+} + \vec{E}_i^{E-}$. These equations are expressed in the (x, y, z) coordinate axis system. Now it is convenient to express the field components in the waveguide coordinate axis system (this system is shown in Figs. 5 and 7). It is worth mentioning that the waveguide coordinate system is defined as a function of the diffracted angle. For the i-order forward-diffracted wave the transformation between the waveguide coordinate system (x_{wi}, y_{wi}, z_{wi}) and the coordinate axis system (x, y, z) is a rotation by $-\delta_i^{pp}$, and the translation along the z axis has been suppressed because does it not affect the results. Using that transformation the the diffracted fields are:

$$\vec{E}_{wi}^{p\pm} = (T_{xwip\pm}\hat{x}_{wi} + T_{ywip\pm}\hat{y}_{wi} + T_{zwip\pm}\hat{z}_{wi})\exp[-jk_0(\pm k_{xwfp}x_{wi} + \beta' z_{wi})], \qquad (32)$$

where $T_{uwip\pm}$ $(u = x, y, z)$ are the complex amplitude components expressed in the (x_{wi}, y_{wi}, z_{wi}) coordinate axis system.

B1. Optic Axis Perpendicular to the Electrode Surface

Using the properties of the ordinary and the extraordinary waves and the geometrical conditions it is straightforward to show for TE modes that

$$\vec{E}_{wi}^{O\pm} = \hat{y}_{wi}T_{ywiO\pm}\exp[-jk_0(\pm k_{xwfO}x_{wi} + \beta' z_{wi})], \qquad (33)$$

and for the TM modes that

$$\vec{E}_{wi}^{E\pm} = [T_{xwiE\pm}\hat{x}_{wi} + T_{zwiE\pm}\hat{z}_{wi}\exp[-jk_0(\pm k_{xwfE}x_{wi} + \beta' z_{wi})]. \qquad (34)$$

Consequently, the i-order diffracted waves of a TE incident mode will constitute a TE mode and i-order diffracted waves of a TM incident mode will constitute a TM mode. It is convenient to compare the diffracted electric fields with the incident electric fields, which are given by Eq. (A5) for a TE mode and by Eqs. (A9) and (A10) for a TM incident mode.

Thus, the complex amplitude ratio coefficients are defined for the TE modes (ordinary waves) as

$$f_{iO+} = |f_{iO+}|\exp(-j\varphi_{iO+}) = \frac{T_{ywiO+}}{F_{O+}}, \tag{35}$$

$$f_{iO-} = |f_{iO-}|\exp(-j\varphi_{iO-}) = \frac{T_{ywiO-}}{F_{O-}}, \tag{36}$$

and for the TM modes (extraordinary waves)

$$f_{iE+} = |f_{iE+}|\exp(-jk_0\varphi_{iE+}) = \frac{T_{xwiE+}}{(\beta'/\epsilon_{zzwf})F_{E+}} = \frac{T_{xwiE+}}{-(k_{xwfE}/n_{Of}^2)F_{E+}}, \tag{37}$$

$$f_{iE-} = |f_{iE-}|\exp(-jk_0\varphi_{iE-}) = \frac{T_{xwiE-}}{(\beta'/\epsilon_{zzwf})F_{E-}} = \frac{T_{xwiE-}}{+(k_{xwfE}/n_{Of}^2)F_{E-}}. \tag{38}$$

The f_{iO+}, f_{iO-}, f_{iE+}, and f_{iE-} coefficients express ratios between incident and diffracted complex amplitude components. Using the above defined coefficients the i-order diffracted total electric field can be written for the TE modes as

$$E_{ywif} = [f_{iO+}F_{O+}a_{O+}(x_{wi}) + f_{iO-}F_{O-}a_{O-}(x_{wi})]a_i(z_{wi}), \tag{39}$$

where $a_{O+}(x_{wi})$ and $a_{O-}(x_{wi})$ were defined previously (as a function of x_w) and $a_i(z_{wi}) = \exp(-jk_0\beta' z_{wi})$. Similar expressions to those of Eqs. (A6) and (A7) can be written for the total magnetic field that corresponds to the i-order. Now for the TM modes the total electric field components for the i-th order are

$$E_{xwif} = \frac{\beta'}{\epsilon_{zzwf}}[f_{iE+}F_{E+}a_{E+}(x_{wi}) + f_{iE-}F_{E-}a_{E-}(x_{wi})]a_i(z_{wi}), \tag{40}$$

$$E_{zwif} = -\frac{k_{xwfE}}{n_{Of}^2}[f_{iE+}F_{E+}a_{E+}(x_{wi}) - f_{iE-}F_{E-}a_{E-}(x_{wi})]a_i(z_{wi}). \tag{41}$$

The complex coefficients f_{iO+}, f_{iO-}, f_{iE+}, and f_{iE-} influence the phase and the amplitude relationship of the plane wave components of the diffracted mode. The mode, however, should satisfy the characteristic mode amplitude and phase relationship for its plane wave components. Thus, only the in-phase waves with the correct amplitude ratios as given by Eq. (39) for the TE modes and by Eqs. (40) and (41) for the TM modes will constitute

the i-th diffracted mode. These phase and amplitude parts of the electric fields for the TE modes are

$$E_{ywij} = f_{iO+}\rho_{TE}[f_{iO+}F_{O+}a_{O+}(x_{wi}) + f_{iO-}F_{O-}a_{O-}(x_{wi})]a_i(z_{wi}), \tag{42}$$

and for the TM modes are

$$E_{zwij} = \frac{\beta' f_{iE+}\rho_{TM}}{\epsilon_{zzwj}}[f_{iE+}F_{E+}a_{E+}(x_{wi}) + f_{iE-}F_{E-}a_{E-}(x_{wi})]a_i(z_{wi}), \tag{43}$$

$$E_{xwij} = -\frac{k_{zwjE}f_{iE+}\rho_{TM}}{n_{Oj}^2}[f_{iE+}F_{E+}a_{E+}(x_{wi}) - f_{iE-}F_{E-}a_{E-}(x_{wi})]a_i(z_{wi}), \tag{44}$$

where $\rho_q = min\{1,\ max\{(|f_{iE-}|/|f_{iE+}|)\cos(\varphi_{iE+} - \varphi_{iE-}),\ 0\}\}$, and $q = O,\ E$ (O corresponds to TE modes and E corresponds to TM modes). The coefficients ρ_O and ρ_E satisfy the inequality $0 \leq \rho_O,\ \rho_E \leq 1$, and they represent the radiation losses of the mode due to the phase and amplitude mismatches. For this decoupled optic axis orientation, however, due to the symmetry of the problem $f_{iO+} \simeq f_{iO-}$ for the TE modes and $f_{iE+} \simeq f_{iE-}$ for the TM modes. Consequently, $\rho_O \simeq 1$ and $\rho_E \simeq 1$ which means that in this decoupled case there is negligible radiation loss due to the amplitude and the phase mismatches.

B2. Optic Axis in the Plane of the Electrode Surface

In this case the modes are hybrid and the general equation (32) must be used. Again coefficients f_{iO+}, f_{iO-}, f_{iE+}, and f_{iE-} can be defined as follows

$$f_{ip\pm} = |f_{ip\pm}|\exp(-j\varphi_{ip\pm}) = \frac{T_{zwip/pm}}{\frac{\beta'}{\epsilon_{zzwj}}\frac{k_{zwjp}c_j}{k_{zwjp}^2 - b_j}F_{p\pm}} =$$

$$= -\frac{T_{ywip\pm}}{F_{p\pm}} = \frac{T_{zwip\pm}}{\frac{a_j}{k_{zwjp}^2 - b_j}F_{ip\pm}}, \tag{45}$$

where $p = O,\ E$. Using a similar procedure to the one above for the TE and TM modes, the following electric field components, that satisfy the phase and amplitude conditions,

can be written

$$E_{xwij} = \sum_{q=O,E} \frac{\beta' k_{xwfq} f_{iO+} \rho}{\varepsilon_{xxwf}} [F_{q+} a_{q+}(x_{wi}) - F_{q-} a_{q-}(x_{wi})] a_i(z_{wi}), \tag{46}$$

$$E_{ywij} = \sum_{q=O,E} f_{iO+} \rho [F_{q+} a_{q+}(x_{wi}) + F_{q-} a_{q-}(x_{wi})] a_i(z_{wi}), \tag{47}$$

$$E_{zwij} = \sum_{q=O,E} \frac{a_f f_{iO+} \rho}{k^2_{xwfq} - b_f} [F_{q+} a_{q+}(x_{wi}) + F_{q-} a_{q-}(x_{wi})] a_i(z_{wi}), \tag{48}$$

where

$$\rho = min\{1,\ max\{\frac{|f_{iO-}|}{|f_{iO+}|}\cos(\varphi_{iO-} - \varphi_{iO+}),\ 0\},\ max\{\frac{|f_{iE+}|}{|f_{iO+}|}\cos(\varphi_{iE+} - \varphi_{iO+}),\ 0\},$$
$$max\{\frac{|f_{iE-}|}{|f_{iO+}|}\cos(\varphi_{iE-} - \varphi_{iO+}),\ 0\}\}. \tag{49}$$

Again the coefficient ρ is related to the radiation losses due to the phase and amplitude mismatches of the plane waves and satisfies the inequality $0 \leq \rho \leq 1$. Similar expressions to Eqs. (46)–(48) can be written for the magnetic fields. Figure 9 demonstrates the general relation of the complex coefficients f_{iO+}, f_{iO-}, f_{iE+}, and f_{iE-}, in the complex plane.

If $\rho = 0$, which is a possible situation, then the diffracted mode will be coupled to radiation modes only. In the following section some comments on the diffracted mode efficiencies are discussed.

VII. Mode Diffraction Efficiencies

In order to determine the efficiencies of the diffracted modes it is important to compute the power per unit area, along the x_{wi} and y_{wi} coordinates, that propagates in the z_{wi} direction. The power per unit area can be found at any point using the components of the Poynting vector. Then, the power per unit area that is propagating in the z_{wi} direction can be found by a simple integration

$$P_{xwij} = \int_0^d S_{xwij}(x_{wi}) dx_{wi}, \tag{50}$$

where P_{zwif} is the power per unit area in the z_{wi} direction and S_{zwif} is the z_{wi} component of the Poynting vector as given in Appendix C. Both P_{zwif} and S_{zwif} correspond to the film region only. The power in the cover and the substrate can be computed similarly, but since it was assumed that the evanescent fields in the cover and the substrate regions follow the same diffraction characteristics as the corresponding plane waves, the expressions for the film region power will be generalized for the total power propagating along the z_{wi} direction of the waveguide.

The power per unit area along the z_{wi} direction can be found using Eq. (50). The efficiency of a diffracted mode, DE_i, can be defined as

$$DE_i = \frac{P_{zwif}}{P_{zwf}} = \rho^2 |f_{iq+}|^2 \frac{\cos \delta_i^{qq}}{\cos \delta}, \tag{51}$$

where P_{zwf} is the incident power per unit area and $q = O,\ E$. If $q = O$, Eq. (51) gives the diffraction efficiency of a pure TE mode while if $q = E$ it gives the diffraction efficiency of a TM mode. For the hybrid mode case $\delta_i^{OO} = \delta_i^{EE} = \delta_i$ and $q = O$.

VIII. Diffraction by Slanted Electrode Configurations

In this section the diffraction of guided waves in anisotropic dielectric slab waveguides by slanted-interdigitated-electrode induced phase gratings will be discussed. Again the mode propagation conditions described in section VI should hold. The *amplitude/phase* conditions do not change in the case of slanted electrodes and the analysis presented in subsection VI.B is still valid under the same given conditions of section I. There are, however, some differences in the *geometrical* conditions that will be identified for the two optic axis orientations of interest.

A. Optic Axis Perpendicular to the Electrode Surface

Due to the cylindrical symmetry of the wavevector surfaces (along the z axis), all

the geometrical conditions are still satisfied, and Eqs. (21)–(24) are valid. In this case, however, $K_x = K \sin\phi$, where ϕ is the slant angle of the induced grating. Again, two distinct decoupled mode types can be identified, TE and TM modes. In Fig. 10 the xy plane wavevector intersections are shown for a TE mode (Fig. 10a) and for a TM mode (Fig. 10b). The cylindrical symmetry for both modes types does not affect the geometrical conditions of the problem. The Bragg conditions are given by $\Lambda_q = \lambda_0 i / 2\beta'_q \cos(\phi - \delta)$, where $q = O$, E, for the two ordinary or the two extraordinary waves of the incident mode.

B. Optic Axis in the Plane of the Electrode Surface

This is the case of a hybrid incident mode where both ordinary and extraordinary homogeneous plane waves are incident. Multiple Bragg conditions and diffraction directions are possible similar to those shown in Fig. 7. Equations (25)–(28) hold again if $K_x = K \sin\phi$. In order to satisfy the geometrical conditions, a restriction in the orientation of the optic axis is required. It can be easily shown that when the optic axis is parallel or perpendicular to the grating vector orientation and the Bragg condition is satisfied then

$$k_{y_i}^{OO} = k_{y_i}^{EE} = \pm\beta' \cos(2\phi - \delta - \pi), \tag{52}$$

and the four homogeneous plane wave components lie in the same vertical plane at an angle $\delta_i^{OO} = \delta_i^{EE} = 2\phi - \delta - \pi$ and the same propagation constant β'. The sign in Eq. (52) should be chosen such that $k_{y_i}^{OO} = k_{y_i}^{EE} < 0$ (propagation along the $-y$ direction). Consequently, when the optic axis is parallel or perpendicular to the grating vector and at Bragg incidence the first geometrical condition is satisfied. The second condition is also satisfied since Eq. (30) holds for $2\phi - \delta - \pi$ also, as can be shown using the same propagation constant β'. Finally, the third geometrical condition is also satisfied and all the ordinary and extraordinary incident plane waves share the same Bragg condition given as before (for $\beta'_q = \beta'$). Plane intersections of the wavevector surfaces are shown in Fig. 11 for the optic axis parallel to the grating vector (Fig. 11a) and for the optic axis perpendicular to

the grating vector (Fig. 11b).

IX. Multiple Slanted Electrode Configurations

It is relatively straightforward to generalize the above results for the case of multiple cascaded gratings. The *amplitude/phase* conditions remain unaffected if the multiple cascaded anisotropic grating diffraction analysis described in Ref. 58 is used. The geometrical conditions in the case of the optic axis being perpendicular to the electrode surface are again satisfied due to the cylindrical symmetry of the wavevector surfaces (along the z axis). Consequently, any cascaded configuration of electrodes can be treated without restrictions if the optic axis is perpendicular to the electrode surface. In addition, if the optic axis lies in the electrode plane then the grating vector should be parallel or perpendicular to the electrode surface and if ϕ_ℓ and $\phi_{\ell+1}$ are the slant angles of two consequetive gratings then $|\phi_\ell - \phi_{\ell+1}| = 0$, or $\pi/2$. An additional constraint is that the multiple type Bragg conditions must hold in order to satisfy all the geometrical conditions. Summarizing, the hybrid mode case is much more restrictive than decoupled cases due to the differing diffraction characteristics of the ordinary and extraordinary waves.

X. Lithium Niobate Example

In this section two examples of guided wave anisotropic diffraction analyses are described. Those examples are based on two applications of lithium niobate interdigitated electrode devices. These applications are: a Givens rotation device and a herringbone multiplier. In both of these examples the optic axis orientation is chosen to be perpendicular to the electrode surface. This configuration, as will be justified later, is the most efficient if the waveguide is designed to support only the TM_0 mode. This can be achieved if the change in the extraordinary film index is greater than the change of the ordinary film index comparing these indices with the corresponding substrate indices. In all the examples the

film and substrate material is lithium niobate while the cover is silicon dioxide which serves as a buffer layer between the electrodes and the waveguide. The superstrate is air. The operating freespace wavelength is taken to be $1.0\mu m$ and the refractive indices (at that wavelength) are $n_c = 1.51$, $n_{Of} = 2.2512$, $n_{Ef} = 2.1894$, $n_{Os} = 2.2362$, and $n_{Es} = 2.1594$. These indices correspond to a titanium diffusion formed waveguide. The film thickness is taken to be $1.0\mu m$. Solving the waveguiding problem using Eq. (3) for TE modes or TM modes (due to the decoupled orientation of the optic axis that equation may be greatly simlified as was described in section II.A). For the chosen film thickness only TE_0 and TM_0 modes can propagate with normalized propagation constants of $\beta'_{TE} = 2.2367$ and $\beta'_{TM} = 2.1671$. The x_w normalized components of the ordinary or extraordinary wavevectors of the plane wave mode components can be found using Eq. (B6) or (B7) respectively of Appendix B. The induced relative permittivity tensor under the electrodes (inside the waveguide) depends on the chosen periodicity of the grating (or equivalently the electrode spacing), the thickness of the buffer layer, the ratio of the electrode width to electrode spacing (which in all the examples is $w/\Lambda_e = 0.50$), and the ratio of the electrode thickness to the electrode spacing. In addition, the electrostatic relative permittivities are $\epsilon_c = 3.90$ (SiO_2), and $\epsilon_{xx4} = \epsilon_{yy4} = 84.142$ and $\epsilon_{zz4} = 28.122$ (lithium niobate). The relative permittivity of the air is assumed to be unity. The small difference in the relative permittivities of the film and the substrate regions is negligible in the analysis of the electrostatic problem.

A. Givens Rotation Device Example

The Givens rotation operation occupies a central role in linear algebraic signal processing. An integrated-optical coherent implementation of an elementary rotation matrix device, can be constructed based on a thick grating induced by interdigitated-electrodes. Consequently, the same device that has been described in the previous subsection can be used as a Givens rotation device[23] to implement the Givens orthogonalization. However,

in this case the *amplitude* of the transmitted and diffracted fields is needed for correct operation. The transmitted field must vary as $\sin(K_v V)$ and the diffracted field as $\cos(K_v V)$ where K_v is a constant and V is the voltage applied to the interdigitated electrodes.

The Givens rotation device is shown schematically in Fig. 12. The periodicity of the induced grating (and consequently the electrode spacing) is such that it satisfies the first Bragg condition for a TM_0 incident mode. Using the normalized propagation constant $\beta'_{TM} = 2.1671$ for an angle of incidence $\delta = 5°$, a Bragg periodicity of $\Lambda_{TM} = \Lambda_O = 2.6473\mu m$ can be computed. For a film thickness of $1.0\mu m$ a TE_0 mode can also propagate. However, the coupling between $TM_0 - TE_0$ is negligible since the deviation from the Bragg periodicity can easily be computed from the equation,

$$\beta'^2_{TE} = \beta'^2_{TM} + m^2\frac{K^2}{k_0^2} - 2m\frac{K}{k_0}\beta'_{TM}\cos\left(\frac{\pi}{2} - \delta\right), \tag{53}$$

and is found to be $0.25\mu m$ which is very large for "thick" grating diffraction. The buffer layer thickness is $d_c = 0.25\mu m$, and the electrode thickness is $2t = 0.10\mu m$. Using the analysis described in Ref. 57 the relative permittivity tensor can be calculated and is $\epsilon_{11} = -0.39 \times 10^{-4}\ V/\mu m$, $\epsilon_{33} = -1.14 \times 10^{-4}\ V/\mu m$, $\epsilon_{12} = -0.15 \times 10^{-4}\ V/\mu m$, $\epsilon_{13} = 0.69 \times 10^{-4}\ V/\mu m$, and the $g_1^{eq} \simeq 0.24$ computed with averaging along the z direction of the electric field without any optical weighting.

The 0-order and the +1-order forward-diffracted electric fields are shown in Fig. 13 as a function of the applied voltage normalized with respect to the incident electric field. The dotted lines correspond to rigorous calculations using the analysis described in this chapter, while the continuous lines correspond to a cosine, $\cos(K_v V)$, (Fig. 13a) or a sine, $\sin(K_v V)$, (Fig. 13b) best fit on the rigorously computed results. The best fit value for K_v was 0.123 rad/volt. The agreement between the rigorous curves (dotted lines) and the cosine and sine approximations (continuous curves) is excellent. This good agreement is necessary for the correct device operation.

B. Herringbone Multiplier Example

Similarly to the previously described case, a Z-cut (optic axis along the z direction) slab is used for the design of the herringbone multiplier. It is taken that the TM_0 mode is propagating. The angle of incidence is $\delta = -5°$ (Fig. 1a). The TM_0 mode consists of two extraordinary polarized plane waves with parameters that can be computed by Eq. (B7), where again $\beta' = \beta'_{TM} = 2.1671$. The slant angle of the first grating, ϕ_1, can be computed using Ref. 58 for $i_1 = i_2 = 1$ to be $\phi_1 = 87.5°$. Another solution of the same equation is $\phi_1 = -2.5°$ which corresponds to a backward diffracting grating and consequently is not practical for the design of the multiplier. The slant angle of the second grating is $\phi_2 = 92.5°$ (again using the equations of Ref. 58). The common periodicity Λ of both gratings can be calculated to be $5.3\mu m$. The thicknesses of both gratings were chosen to be equal, $s_1 = s_2 = 1000\mu m$. The top-view of the multiplier and the corresponding wavevector diagram are shown in Figs. 14a and 14b respectively. For the electrostatic analysis the ratio of the electrode gap to the electrode spacing is $\ell/\Lambda_e = 0.5$ (where Λ_e is the electrode spacing). The buffer layer is assumed to be $0.15\mu m$ and the electrode thickness $0.25\mu m$. Using the electrostatic analysis of Ref. 57 the fundamental component of the electric potential Q_1 is found to be 0.3146 volts. The induced permittivities are

$$\begin{aligned}
\varepsilon_{xxk} &= [\varepsilon_{11k}\cos(\vec{K}_\ell \cdot \vec{r}) + \varepsilon_{22k}\sin(\vec{K} \cdot \vec{r})](V_k/\Lambda_{ek}),\\
\varepsilon_{yyk} &= [-\varepsilon_{11k}\cos(\vec{K}_\ell \cdot \vec{r}) + \varepsilon_{22k}\sin(\vec{K} \cdot \vec{r})](V_k/\Lambda_{ek}),\\
\varepsilon_{zzk} &= \varepsilon_{33k}[\sin(\vec{K}_\ell \cdot \vec{r})](V_k/\Lambda_{ek}),\\
\varepsilon_{xyk} &= \varepsilon_{12k}[\cos(\vec{K}_\ell \cdot \vec{r})](V_k/\Lambda_{ek}),\\
\varepsilon_{xzk} &= \varepsilon_{13k}[\cos(\vec{K}_\ell \cdot \vec{r})](V_k/\Lambda_{ek}),\\
\varepsilon_{yzk} &= \varepsilon_{23k}[\cos(\vec{K}_\ell \cdot \vec{r})](V_k/\Lambda_{ek}),
\end{aligned} \tag{54}$$

where $k = 1, 2$, $\varepsilon_{111} = 0.32 \times 10^{-5}\ V/\mu m$, $\varepsilon_{112} = -\varepsilon_{111}$, $\varepsilon_{221} = \varepsilon_{222} = -0.19 \times 10^{-3}\ V/\mu m$, $\varepsilon_{331} = \varepsilon_{332} = -0.54 \times 10^{-3}\ V/\mu m$, $\varepsilon_{121} = \varepsilon_{122} = -0.72 \times 10^{-4}\ V/\mu m$, $\varepsilon_{131} = \varepsilon_{132} = 0.32 \times 10^{-3}\ V/\mu m$, $\varepsilon_{231} = -\varepsilon_{232} = -0.14 \times 10^{-4}\ V/\mu m$, $g_1^{ee} = 0.43$, and V_1, V_2 are the applied voltages. In order to operate the multiplier it is a requirement to have

an output which is proportional to the product of the two applied voltages $V_1 V_2$. Thus, the desired diffraction efficiency is of the form $DE \simeq K_* V_1 V_2$.

The performance of the multiplier has been evaluated with a numerical example. In order to achieve better performance a set of bias voltages have been added. The bias voltages V_{b1}, V_{b2} were chosen 10.8 volts in order to operate as close as possible to the linear response of the diffraction curves of each grating. The input voltages V_1, V_2 were varied around the bias voltages in the range from 8.8 volts to 12.8 volts. The -2-order forward-diffracted mode efficiency is shown in Fig. 15 as a function of the voltage $V = V_1 = V_2$, along with the predicted efficiency from the equation $DE_{pr} = K_* V_1 V_2$ (where K_* has been computed around the bias point to be $(0.25/10.8^2)$ 1/volt^2). The error as a function of the applied input voltage is also shown in Fig. 15. The percentage error has been calculated using the formula $PE = (DE_{pr} - DE) \times 100/DE$ where DE is the rigorously computed efficiency and DE_{pr} is the predicted efficiency using the equation $DE_{pr} = K_* V_1 V_2$. It is observed that the error is in the order of $\pm 8\%$ for the chosen range of variation of the input voltages around the bias points. One potential problem of the proposed multiplier is the limited dynamic range if larger voltages are necessary. Consequently, compensating electronics may be necessary.

XI. Hybrid Mode Example

In this hybrid mode case the lithium niobate crystal is assumed to be Y-cut and X propagating. Consequently, the optic axis is along the x axis of the coordinate axis system that is used in this analysis. The refractive indices of the cover, film and substrate are $n_c = 1.51$, $n_{Of} = 2.254$, $n_{Ef} = 2.174$, $n_{O*} = 2.234$, and $n_{E*} = 2.154$, at an operating freespace wavelength of $\lambda_0 = 1.06\mu m$. The thickness of the film region is again assumed to be $1.0\mu m$. According to Eq. (6), in order to have four homogeneous plane wave components the angle of incidence δ should be greater than a critical angle which for the given parameters of

the waveguide is 60.7°. In this analysis the angle of incidence is chosen to be $\delta = 62°$ and therefore is greater than the critical angle. Using the above defined parameters and the analysis of Refs. 59 and 60 [or Eq. (8)], two acceptable values of the normalized propagation constant $\beta' = 2.217$, and $\beta' = 2.235$ are calculated. From these values only $\beta' = 2.235$ corresponds to four homogeneous plane wave mode components. Using Eqs. (B6) and (B7) of Appendix B all the plane wave parameters can be computed. From the Bragg condition $\Lambda = 0.27\mu m$. This periodicity is very small for practical applications due to the large angle of incidence but the results of this example analysis are only for demonstration of the hybrid mode effects. Using a buffer layer of $0.05\mu m$ and $\ell/\Lambda_e = 0.5$, a fundamental electric potential harmonic of $Q_1 = 0.054$ volts was computed. The induced permittivity tensor is

$$\begin{aligned}
\varepsilon_{xx} &= \varepsilon_{11}[\cos(Kx)](V/\Lambda_e), \\
\varepsilon_{yy} &= [-\varepsilon_{22}\cos(Kx) - \varepsilon_{33}\sin(Kx)](V/\Lambda_e), \\
\varepsilon_{zz} &= [\varepsilon_{22}\cos(Kx) - \varepsilon_{33}\sin(Kx)](V/\Lambda_e), \\
\varepsilon_{xy} &= \varepsilon_{yz} = 0, \\
\varepsilon_{xz} &= \varepsilon_{13}[\sin(Kx)](V/\Lambda_e),
\end{aligned} \tag{55}$$

where $\varepsilon_{11} = 0.61 \times 10^{-4}\ V/\mu m$, $\varepsilon_{22} = 0.22 \times 10^{-4}\ V/\mu m$, $\varepsilon_{33} = 0.85 \times 10^{-4}\ V/\mu m$, $\varepsilon_{13} = -0.38 \times 10^{-4}\ V/\mu m$, and $g_1^{eq} \simeq 0.5$. The grating thickness was assumed to be $2000\mu m$, and the applied voltage was varied between 0 and 50 volts. The diffraction efficiencies of the $O+$, $O-$, $E+$, and $E-$ waves are shown in Fig. 16 and their corresponding phases in Fig. 17 (for the 0-order and the Bragg-order) as a function of the applied on the electrodes voltage. The resulting mode efficiencies are shown in Fig. 18 for the 0-order (dashed line) and the Bragg-order (continuous line). It is shown that the diffracted mode efficiencies in this case appear to have significant radiation losses due to the phase and amplitude mismatch between the ordinary and the extraordinary waves.

XII. Comparison with Experimental Results

In this section the results of the analysis presented are compared with the experimental results of Ref. 18. The geometrical configuration is that of Fig. 1. The electrodes are unslanted with respect to the (x, y, z) coordinate system and the optic axis orientation is along the x axis. Before starting the analysis of that configuration it is worthwhile to comment on this optic axis orientation. According to the results of Refs. 59 and 60 for this optic axis orientation, the propagating modes at normal incidence to the grating, are characterized as critically stable. Slight divergence in the angle of incidence from propagation along the $-y$ axis changes the mode from pure TE_0 to a leaky mode. In this leaky mode region, due to the negative crystal birefringence, the ordinary component of the hybrid mode leaks into the substrate.

For the diffraction process it is necessary to use angles of incidence away from the normal. For this propagation direction the modes are leaky guided modes and power will be lost as it travels down the waveguide even if the grating is not present. Additional losses are also present due to the diffraction of the hybrid mode as described previously. In order to study the above experimental configuration the hybrid character of the incident mode will be suppressed due to the very small angle of incidence ($\delta = 0.62°$). Consequently, the leaky character of the mode will also be neglected.

For the electrostatic analysis the ratio ℓ/Λ_e is 0.5, the electrode thickness is $0.5\mu m$, and the buffer layer (SiO_2) thickness is $0.15\mu m$. The grating periodicity Λ is 13.33 μm. The low-frequency relative permittivities of all the materials are the same as in section 5.10. The fundamental harmonic of the electric potential is $Q_1 = 0.54$ volts. Using that value of Q_1 a fundamental electric field harmonic of $E_1 = 0.422(V_E/\ell)$ is computed, where V_E is the voltage difference between two consequetive electrodes. If Engan's analysis is used[18,61] then the corresponding fundamental harmonic is $E_1 = 0.847(V_E/\ell)$. As a result, neglecting the electrode thickness and the buffer layer introduces an error in the electrostatic field

computation of about 50%. Similarly, the error in the capacitance computation is of the same order. The operating freespace wavelength is $0.633\mu m$ and the refractive indices of the film are taken to be $n_{Of} = 2.2885$ and $n_{Ef} = 2.2014$. At normal incidence on the grating the incident mode would be a TE_0 mode. For the given optic axis orientation the TE_0 mode corresponds to two extraordinary incident waves. The normalized propagation constant is found using the Bragg condition given in Ref. 18 and is 2.194. The parameters of the two extraordinary waves can be computed from Eq. (II.7). The induced relative permittivity tensor is given by Eqs. (55) where $\epsilon_{11} = 0.69\times10^{-3}\ V/\mu m$, $\epsilon_{22} = 0.25\times10^{-3}\ V/\mu m$, $\epsilon_{33} = 0.97\times10^{-4}\ V/\mu m$, $\epsilon_{13} = -0.43\times10^{-3}\ V/\mu m$, and $g_1^{eq} = 0.51$. The Bragg diffracted mode efficiency along with the experimental results are shown in Fig. 19. An important difference between the experimental and the theoretical results is that experimental efficiencies are normalized with respect to the output power while the theoretical results are normalized with respect to the input power. This is the reason that the losses do not appear in the experimental data even if it is known that the incident mode is slightly leaky.

XIII. Discussion and Summary

It has been shown that all optic axis orientations supporting only hybrid modes introduce radiation losses after the diffraction process due to the geometrical and amplitude/phase mismatches of the ordinary and extraordinary waves. In some cases (leaky guided modes) this is true for the mode even without the diffraction by the interdigitated-electrode induced grating.[59, 60] In this paper the most efficient optic axis orientation is identified to be the orientation corresponding to the z axis direction (perpendicular to the electrode surface). This decoupled optic axis orientation guarantees negligible radiation losses due to the different mismatch types. For this preferred orientation of the optic axis the propagation of only the TM_0 mode can be achieved (for negative birefringent lithium niobate) since its cutoff thickness is smaller than that for TE_0 mode. Consequently, the large electrooptic coefficient can also be utilized. An additional advantage is the increase

of the z component of the electrostatic field (that affects the index difference due to the largest electrooptic coefficient in lithium niobate). As a result the orientation of the optic axis perpendicular to the electrode surface should be preferable.

In the case of the hybrid modes the resulting diffraction efficiencies are affected by radiation losses. This is due to the various mismatches of the $O+$, $O-$, $E+$, and $E-$ waves and especially the mismatch between the ordinary and the extraordinary components. However, the analysis neglects the coupling between the different guided or radiation modes. This coupling, in some cases, can act cooperatively with the diffraction process resulting in decreased radiation losses. Consequently, the above hybrid mode results can be considered as a guideline in the design of hybrid mode interdigitated-electrode devices. However, propagation along directions where leaky modes are permittable should be avoided.

In summary, an analysis for treating the diffraction of guided-waves in uniaxial anisotropic slab waveguides has been developed for the first time. The analysis is based on the three-dimensional anisotropic rigorous coupled-wave diffraction analysis and on the decomposition of a guided mode in a uniaxial anisotropic slab waveguide into four homogeneous plane wave components. The latter decomposition restricts the types of the guided modes that can be treated to pure guided modes which are decomposable into four homogeneous plane wave components. However, the analysis for the first time takes into account the anisotropic properties of all media, an arbitrary number of diffracted orders, and the noncollinear character of the diffraction (where the incident mode and the grating vectors are not collinear). Example analyses have been presented. These include a Givens rotation device, a herringbone multiplier, and a hybrid mode device. Comparison with experimental data has also been included. The agreement with the experiment simultaneously verifies both the electrostatic analysis and the diffraction analysis. Finally, an efficient configuration for crystals like lithium niobate has been identified along with the propagating mode direction, for electrooptic applications involving grating diffraction and propagating guided-modes in uniaxial anisotropic waveguides.

APPENDIX A:

BOUNDARY CONDITIONS AND FIELD EXPRESSIONS

The matrix $\tilde{A}_i$ of Eq. (1) is

$$\tilde{A}_i = \begin{pmatrix} 0 & 1 & 0 & 0 \\ \varepsilon_{yyi} - \dfrac{\varepsilon_{xyi}^2}{\varepsilon_{xxi}} - \beta'^2 & 0 & \varepsilon_{yxi} - \dfrac{\varepsilon_{xyi}\varepsilon_{xxi}}{\varepsilon_{xxi}} & \dfrac{\varepsilon_{xyi}}{\varepsilon_{xxi}}\beta' \\ -\dfrac{\varepsilon_{xyi}}{\varepsilon_{xxi}}\beta' & 0 & -\dfrac{\varepsilon_{xxi}}{\varepsilon_{xxi}}\beta' & \dfrac{\beta'^2}{\varepsilon_{xxi}} - 1 \\ \dfrac{\varepsilon_{xyi}\varepsilon_{xxi}}{\varepsilon_{xxi}} - \varepsilon_{yxi} & 0 & \dfrac{\varepsilon_{xxi}^2}{\varepsilon_{xxi}} - \varepsilon_{xxi} & -\dfrac{\varepsilon_{xxi}}{\varepsilon_{xxi}}\beta' \end{pmatrix}, \qquad \text{(A1)}$$

where $i = c,\ f,\ s$.

The boundary conditions of the anisotropic slab waveguide of Fig. 2 are:

(a) Film-substrate interface ($x_w = 0$)

$$\tilde{W}_f \tilde{C}_f = \tilde{W}_s \tilde{C}_s, \qquad \text{(A2)}$$

where the unknown constant matrices are of the form $\tilde{C}_f = [F_{O+},\ F_{E+},\ F_{O-},\ F_{E-}]^T$ and $\tilde{C}_s = [0,\ 0,\ S_{O-},\ S_{E-}]^T$.

(b) Film-cover interface ($x_w = d$)

$$\tilde{W}_f [\exp(-jk_0 \tilde{\Lambda}_f d)] \tilde{C}_f = \tilde{W}_c \tilde{C}_c, \qquad \text{(A3)}$$

where $\tilde{C}_c = [C_{O+},\ C_{E+},\ 0,\ 0]^T$ and the matrix $\tilde{C}_c$ was shifted by $\exp(+jk_0 \tilde{\Lambda}_c d)$ in Eq. (2) for simplicity in the resulting boundary conditions. Combining Eqs. (A2) and (A3) the following condition must be satisfied

$$\begin{pmatrix} C_{O+} \\ C_{E+} \\ 0 \\ 0 \end{pmatrix} = \{\tilde{W}_c^{-1} \tilde{W}_f [\exp(-jk_0 \tilde{\Lambda}_f d)] \tilde{W}_f^{-1} \tilde{W}_s\} \begin{pmatrix} 0 \\ 0 \\ S_{O-} \\ S_{E-} \end{pmatrix}, \qquad \text{(A4)}$$

where for simplification in the notation $\tilde{W}_c^{-1} \tilde{W}_f [\exp(-jk_0 \tilde{\Lambda}_f d)] \tilde{W}_f^{-1} \tilde{W}_s = \tilde{P}(\beta')$.

Using Eq. (2) and the other Maxwell's equations it can be shown that the field expressions in the film region for a TE mode are

$$E_{ywf} = [F_{O+}\, a_{O+}(x_w) + F_{O-}\, a_{O-}(x_w)] \exp(-jk_0\beta' z_w), \tag{A5}$$

$$\eta_0 H_{xwf} = k_{xwfO}[F_{O+}\, a_{O+}(x_w) - F_{O-}\, a_{O-}(x_w)] \exp(-jk_0\beta' z_w), \tag{A6}$$

$$\eta_0 H_{zwf} = -\beta'[F_{O+}\, a_{O+}(x_w) + F_{O-}\, a_{O-}(x_w)] \exp(-jk_0\beta' z_w), \tag{A7}$$

$$E_{xwf} = E_{zwf} = \eta_0 H_{ywf} = 0, \tag{A8}$$

where $a_{O+}(x_w) = \exp(-jk_0 k_{xwfO} x_w)$, and $a_{O-}(x_w) = \exp(+jk_0 k_{xwfO} x_w)$. Similarly to the TE mode case the fields in the film region for a TM mode are

$$E_{zwf} = \frac{\beta'}{\epsilon_{zzwf}} [F_{E+}\, a_{E+}(x_w) + F_{E-}\, a_{E-}(x_w)] \exp(-jk_0\beta' z_w), \tag{A9}$$

$$E_{xwf} = -\frac{k_{xwfE}}{n_{Of}^2} [F_{E+}\, a_{E+}(x_w) - F_{E-}\, a_{E-}(x_w)] \exp(-jk_0\beta' z_w), \tag{A10}$$

$$\eta_0 H_{ywf} = [F_{E+}\, a_{E+}(x_w) + F_{E-}\, a_{E-}(x_w)] \exp(-jk_0\beta' z_w), \tag{A11}$$

$$E_{ywf} = \eta_0 H_{zwf} = \eta_0 H_{xwf} = 0, \tag{A12}$$

where $a_{E+}(x_w) = \exp(-jk_0 k_{xwfE} x_w)$, and $a_{E-}(x_w) = \exp(+jk_0 k_{xwfE} x_w)$.

APPENDIX B:

PARAMETERS OF THE GUIDANCE CONDITION WHEN OPTIC AXIS LIES IN THE ELECTRODE PLANE

The parameters appearing in Eq. (8) are:

$$F_{Oq} = \left\{ \left(\Delta_O - \frac{\Delta_{OE}}{k_{xwsq}^2 - b_s} \frac{a_s}{a_f} \right)^2 + \left[\left(\Delta_O - \frac{\Delta_{OE}}{k_{xwsq}^2 - b_s} \frac{c_s}{c_f} \right) \frac{|k_{xwsq}|}{k_{xwfO}} \right]^2 \right\}^{1/2} \tag{B1}$$

$$F_{Eq} = \left\{ \left(\Delta_E + \frac{\Delta_{OE}}{k_{xwsq}^2 - b_s} \frac{a_s}{a_f} \right)^2 + \left[\left(\Delta_E + \frac{\Delta_{OE}}{k_{xwsq}^2 - b_s} \frac{c_s}{c_f} \right) \frac{|k_{xwsq}|}{k_{xwfE}} \right]^2 \right\}^{1/2} \tag{B2}$$

where $q = O, E$ and

$$\Delta_O = \frac{1}{2} \frac{k_{xwfO}^2 - b_f}{k_{xwfO}^2 - k_{xwfE}^2}, \tag{B3}$$

$$\Delta_E = -\frac{1}{2}\frac{k_{zwfE}^2 - b_f}{k_{zwfO}^2 - k_{zwfE}^2}, \tag{B4}$$

$$\Delta_{OE} = \frac{1}{2}\frac{(k_{zwfO}^2 - b_f)(k_{zwfE}^2 - b_f)}{k_{zwfO}^2 - k_{zwfE}^2}, \tag{B5}$$

and $a_p = -(1 - \beta'^2/\epsilon_{zzwp})\epsilon_{yzwp}$, $b_p = (1 - \beta'^2/\epsilon_{zzwp})\epsilon_{zzwp}$, $c_p = \epsilon_{yzwp}$, and $p = c, f, s$ (corresponds to cover, film and substrate regions respectively). The normalized wavevector components k_{zwc}, k_{zwfO}, k_{zwfE}, k_{zwfO}, and k_{zwfE} can be found using the wavevector surface equations. The ordinary components can be found from the equation

$$k_{zwpO}^2 + \beta'^2 - n_{Op}^2 = 0, \qquad p = c,\ f,\ s. \tag{B6}$$

Because of inequalities (4) and (5) the components in the cover and the substrate are pure imaginary and their sign should be chosen in order to have exponentially decaying fields in these regions. The extraordinary components that appear in the film and the substrate regions are given by the extraordinary wavevector surface equation

$$n_{Op}^2(k_{zwpE}^2 + \beta'^2) + (n_{Ep}^2 - n_{Op}^2)c_{zw}^2\beta'^2 - n_{Op}^2 n_{Ep}^2 = 0, \quad p = f,\ s, \tag{B7}$$

where c_{zw} is the direction cosine of the optic axis along the waveguide z_w coordinate axis. The substrate component, because of inequality (4), is pure imaginary and special attention should be taken in the choice of its sign in order to have exponentially decaying fields in the substrate.

The parameters ϕ_{pq} where $p,\ q = O,\ E$ are

$$\phi_{Oq} = \tan^{-1}\left\{-\frac{\Delta_O - [\Delta_{OE}/(k_{zwfq}^2 - b_s)](c_s/c_f)}{\Delta_O - [\Delta_{OE}/(k_{zwfq}^2 - b_s)](a_s/a_f)}\frac{|k_{zwfq}|}{k_{zwfO}}\right\} \tag{B8}$$

$$\phi_{Eq} = \tan^{-1}\left\{-\frac{\Delta_E + [\Delta_{OE}/(k_{zwfq}^2 - b_s)](c_s/c_f)}{\Delta_E + [\Delta_{OE}/(k_{zwfq}^2 - b_s)](a_s/a_f)}\frac{|k_{zwfq}|}{k_{zwfE}}\right\} \tag{B9}$$

where $q = O,\ E$, and the rest of the parameters have been previously defined. The parameters $G_O, G_E, H_O, H_E, g_O, g_E, h_O, h_E, \alpha_O$, and α_E are, $G_q = (1/2)[1 + k_{zwfq}^2/|k_{zwc}|^2]^{1/2}$, $g_q = \tan^{-1}(k_{zwfq}/|k_{zwc}|)$, $H_q = [c_f^2 k_{zwfq}^2 + a_f^2 n_{Oc}^4/|k_{zwc}|^2]^{1/2}/2|k_{zwfq}^2 - b_f|$, $h_q =$

$\tan^{-1}(a_f n_{Oc}^2/c_f k_{zwfq}|k_{zwc}|)$, and $\alpha_q = k_0 k_{zwfq} d$, where $q = O$, E and d is the film thickness.

The expressions for the fields in the film region are

$$E_{zwf} = \sum_{q=O,E} \frac{\beta' k_{zwfq}}{\varepsilon_{zzwf}} [F_{q+} a_{q+}(x_w) - F_{q-} a_{q-}(x_w)] \exp(-jk_0\beta' z_w), \tag{B10}$$

$$E_{ywf} = \sum_{q=O,E} [F_{q+} a_{q+}(x_w) + F_{q-} a_{q-}(x_w)] \exp(-jk_0\beta' z_w), \tag{B11}$$

$$E_{zwf} = \sum_{q=O,E} \frac{a_f}{k_{zwfq}^2 - b_f} [F_{q+} a_{q+}(x_w) + F_{q-} a_{q-}(x_w)] \exp(-jk_0\beta' z_w), \tag{B12}$$

$$\eta_0 H_{zwf} = -\beta' \sum_{q=O,E} [F_{q+} a_{q+}(x_w) + F_{q-} a_{q-}(x_w)] \exp(-jk_0\beta' z_w), \tag{B13}$$

$$\eta_0 H_{ywf} = \sum_{q=O,E} \frac{k_{zwfq} c_f}{k_{zwfq}^2 - b_f} [F_{q+} a_{q+}(x_w) - F_{q-} a_{q-}(x_w)] \exp(-jk_0\beta' z_w), \tag{B14}$$

$$\eta_0 H_{zwf} = \sum_{q=O,E} k_{zwfq} [F_{q+} a_{q+}(x_w) - F_{q-} a_{q-}(x_w)] \exp(-jk_0\beta' z_w), \tag{B15}$$

The expressions for the B_O, B_E, ϑ_O and ϑ_E that appear in the expressions for F_{O+}, F_{O-}, F_{E+}, and F_{E-} in the case of the optic axis lying in the plane of the electrodes are

$$B_O = [(F_{OO}\cos\phi_{OO} - F_{OE} Q \cos\phi_{OE})^2 + (F_{OO}\sin\phi_{OO} - F_{OE} Q \sin\phi_{OE})^2]^{1/2}, \tag{B16}$$

$$B_E = [(F_{EO}\cos\phi_{EO} - F_{EE} Q \cos\phi_{EE})^2 + (F_{EO}\sin\phi_{EO} - F_{EE} Q \sin\phi_{EE})^2]^{1/2}, \tag{B17}$$

$$\vartheta_O = \tan^{-1}\left\{\frac{F_{OO}\sin\phi_{OO} - F_{OE} Q \sin\phi_{OE}}{F_{OO}\cos\phi_{OO} - F_{OE} Q \cos\phi_{OE}}\right\}, \tag{B18}$$

$$\vartheta_E = \tan^{-1}\left\{\frac{F_{EO}\sin\phi_{EO} - F_{EE} Q \sin\phi_{EE}}{F_{EO}\cos\phi_{EO} - F_{EE} Q \cos\phi_{EE}}\right\}, \tag{B19}$$

and,

$$Q = \frac{H_O F_{OO}\sin(\alpha_O - h_O + \phi_{OO}) + H_E F_{EO}\sin(\alpha_E - h_E + \phi_{EO})}{H_O F_{OE}\sin(\alpha_O - h_O + \phi_{OE}) + H_E F_{EE}\sin(\alpha_E - h_E + \phi_{EE})}. \tag{B20}$$

APPENDIX C:

POYNTING VECTOR COMPONENTS

1. Optic Axis Perpendicular to the Electrode Surface

The z_{wi} component of the Poynting vector for this optic axis orientation is

$$S_{zwij} = \frac{\beta' A_O^2}{\eta_0}[1 + \cos(2k_0 k_{zwjO} x_{wi} + 2\phi_{j,O})]|f_{iO+}|^2 \rho^2 |S_{O-}|^2, \qquad \text{(C1)}$$

for the TE modes, and

$$S_{zwij} = \frac{\beta' A_E^2}{\eta_0 \epsilon_{zzwj}}[1 + \cos(2k_0 k_{zwjE} x_{wi} + 2\phi_{j,E})]|f_{iE+}|^2 \rho^2 |S_{E-}|^2, \qquad \text{(C2)}$$

for the TM modes [where $\eta_0 = (\mu_0/\epsilon_0)^{1/2}$].

2. Optic Axis in the Plane of the Electrode Surface

For this case the z_{wi} component of the Poynting vector is

$$\begin{aligned} S_{zwij} = \frac{\beta'}{\eta_0}\{ & B_O^2\left(1 + \frac{C_O^2}{\epsilon_{zzwj}}\right) + B_E^2\left(1 + \frac{C_E^2}{\epsilon_{zzwj}}\right) + \\ & B_O^2\left(1 - \frac{C_O^2}{\epsilon_{zzwj}}\right)\cos(2k_0 k_{zwjO} x_{wi} + 2\vartheta_O) + \\ & B_E^2\left(1 - \frac{C_E^2}{\epsilon_{zzwj}}\right)\cos(2k_0 k_{zwjE} x_{wi} + 2\vartheta_E) + \\ & 4B_O B_E[\cos(k_0 k_{zwjO} x_{wi} + \vartheta_O)\cos(k_0 k_{zwjE} x_{wi} + \vartheta_E) + \\ & C_O C_E \sin(k_0 k_{zwjO} x_{wi} + \vartheta_O)\sin(k_0 k_{zwjE} x_{wi} + \vartheta_E)]\} \\ & \rho^2 |f_{iO+}|^2 |S_{O-}|^2, \end{aligned} \qquad \text{(C3)}$$

where $C_q = k_{zwjq} c_j/(k_{zwjq}^2 - b_j)$, for $q = O,\ E$.

BIBLIOGRAPHY

1. C. M. Verber, V. E. Wood, R. P. Kenan, and N. F. Hartman, "Large Angle Optical Switching in Waveguides in $LiNbO_3$," *Ferroelectr.*, **10**, 253 (1976).

2. A. Neyer, "Electro-Optic X-Switch Using Single Mode Titanium Lithium Niobate Channel Waveguides," *Electron. Lett.*, **19**, 553 (1983).

3. R. V. Schmidt, and P. S. Cross, "Efficient Optical Waveguide Switch/Modulator," *Opt. Lett.*, **2**, 45 (1978).

4. C. S. Tsai, B. Kim, and F. R. El-Akkari, "Optical Channel Waveguide Switch and Coupler Using Total Internal Reflection," *IEEE J. Quantum Electron.*, **QE–14**, 513 (1978).

5. H. Kotani, S. Namba, and M. Kawabe, "Electro-Optic Bragg Deflection Modulators in Corrugated Waveguides," *IEEE J. Quantum Electron.*, **QE–15**, 270 (1979).

6. C. L. Chang, F. R. El-Akkari, and C. S. Tsai, "Fabrication and Testing of Optical Channel Waveguide TIR Switching Networks," *Proc. SPIE*, **269**, 147 (1981).

7. R. C. Alferness, "Waveguide Electro-Optic Modulators," *IEEE Trans. Microwave Theory Tech.*, **MTT–30**, 1121 (1982).

8. O. G. Ramer, "Integrated Optic Electro-Optic Modulator Electrode Analysis," *IEEE J. Quantum Electron.*, **QE–18**, 386 (1982).

9. R. C. Alferness and L. L. Buhl, "Waveguide Electro-Optic Polarization Transformer," *Appl. Phys. Lett.*, **38**, 655 (1981).

10. R. C. Alferness and L. L. Buhl, "Electro-Optic Waveguide TE–TM Mode Converter With Low Drive Voltage," *Opt. Lett.*, **5**, 473 (1980).

11. R. C. Alferness, "Efficient Electro-Optic TE–TM Mode Converter/Wavelength Filter," *Appl. Phys. Lett.*, **36**, 513 (1980).

12. R. C. Alferness, "Guided Wave Devices for Optical Communication," *IEEE J. Quantum Electron.*, **QE–17**, 946 (1981).

13. C. S. Tsai, M. T. Alhaider, N. T. Nguyen, and B. Kim, "Wide-Band Guided Wave Acousto-Optic Bragg Diffraction and Devices Using Multiple Tilted Surface Acoustic Waves," *Proc. IEEE*, **64**, 318 (1976).

14. C. S. Tsai, "Guided-Wave Acousto-Optic Bragg Modulators for Wide Band Integrated Optic Communications and Signal Processing," *IEEE Trans. Circuits Sys.*, **CAS–26**, 1072 (1979).

15. W. T. Rhodes, "Acousto-Optic Signal Processing: Convolution and Correlation," *Proc. IEEE*, **69**, 65 (1981).

16. J. T. Boyd, "Integrated Optoelectronic Silicon Devices for Optical Signal Processing and Communications," *Opt. Eng.*, **18**, 14 (1979).

17. C. M. Verber, R. P. Kenan, and J. R. Busch, "Design and Performance of an Integrated Optical Digital Correlator," *J. Lightwave Technol.*, **LT–1**, 256 (1983).

18. C. M. Verber, R. P. Kenan, and J. R. Busch, "Correlator Based on an Integrated Optical Spatial Light Modulator," *Appl. Opt.*, **20**, 1626 (1981).

19. C. M. Verber, "Integrated-Optical Approaches to Numerical Optical Computing," *Proc. IEEE*, **72**, 942 (1984).

20. C. M. Verber, "Integrated Optical Architectures for Matrix Multiplication," *Opt. Eng.*, **24**, 19 (1985).

21. W. T. Rhodes and P. S. Guilfoyle, "Acousto-Optic Algebraic Processing Architectures," *Proc. IEEE*, **72**, 820 (1984).

22. C. M. Verber and R. P. Kenan, "Integrated Optical Circuits for Numerical Computation," *Proc. SPIE*, **408**, 57 (1983).

23. M. M. Mirsalehi, T. K. Gaylord, and E. I. Verriest, "Integrated Optical Givens Rotation Device," *Appl. Opt.*, **25**, 1608 (1986).

24. C. S. Tsai, D. Y. Zang, and P. Le, "Acousto-Optic Bragg Diffraction in a $LiNbO_3$ Channel-Planar Composite Waveguide with Application to Optical Computing," *Appl. Phys. Lett.*, **47**, 549 (1985).

25. D. Marcuse, "*Theory of Dielectric Optical Waveguides*," (Academic Press, New York, 1974), pp. 95–131.

26. H. Kogelnik, in *Integrated Optics*, **7** of Topics in Applied Physics, T. Tamir, ed. (Springer-Verlag, New York, 1975), pp. 66–79.

27. H. Stoll and A. Yariv, "Coupled-Mode Analysis of Periodic Dielectric Waveguides," *Opt. Commun.*, **8**, 5 1973.

28. A. Yariv, "Coupled-Mode Theory for Guided-Wave Optics," *IEEE J. Quantum Electron.*, **QE–9**, 919 (1973).

29. H. Taylor and A. Yariv, "Guided Wave Optics," *Proc. IEEE*, **62**, 1044 (1974).

30. R. P. Kenan, "Theory of Diffraction of Guided Optical Waves by Thick Holograms," *J. Appl. Phys.*, **46**, 4545 (1975).

31. W. Streifer, D. R. Scifres, and R. D. Burnham, "Coupling Coefficients for Distributed Feedback Single and Double Heterostructure Diode Lasers," *IEEE J. Quantum Electron.*, **QE–11**, 867 (1975).

32. W. Streifer, D. R. Scifres, and R. P. Burnham, "Periodic Corrugated Dielectric Waveguides," *Fiber & Integrated Opt.*, **1**, 63 (1977).

33. K. Wagatsuma, H. Sakaki, and S. Saito, "Mode Conversion and Optical Filtering of Obliquely Incident Waves in Corrugated Waveguide Filters," *IEEE J. Quantum Electron.*, **QE–15**, 632 (1979).

34. A. Hardy and W. Streifer, "Analysis of Waveguided Gaussian Beams Coupled by Misaligned or Curved Gratings," *J. Opt. Soc. Am.*, **69**, 1235 (1979).

35. D. G. Hall, "Diffraction Efficiency of Waveguide Gratings: Brewster's Law," *Opt. Lett.*, **5**, 315 (1980).

36. J. Van Roey and P. E. Lagasse, "Coupled-Wave Analysis of Obliquely Incident Waves in Thin Film Waveguides," *Appl. Opt.*, **20**, 423 (1981).

37. R. W. Cruhlke and D. G. Hall, "Comparison of Two Approaches to the Waveguide Scattering Problem: TM Polarization," *Appl. Opt.*, **23**, 127 (1984).

38. A. Hardy and W. Streifer, "Coupled Modes of Multiwaveguide Systems and Phased Arrays," *IEEE J. Lightwave Technol.*, **LT–4**, 90 (1986).

39. W. Streifer, M. Osiński, and A. Hardy, "Reformulation of the Coupled-Mode Theory of Multiwaveguide Systems," *J. Lightwave Technol.*, **LT–5**, 1 (1987).

40. S. Chuang, "A Coupled-Mode Formulation by Reciprocity and a Variational Principle," *J. Ligthwave Technol.*, **LT–5**, 5 (1987).

41. H. A. Haus, W. P. Huang, S. Kawakami, and N. A. Whitaker, "Coupled-Mode Theory of Optical Waveguides," *J. Ligthwave Technol.*, **LT–5**, 16 (1987).

42. K. Sakuda and A. Yariv, "Analysis of Optical Propagation in a Corrugated Dielectric Waveguide," *Opt. Commun.*, **8**, 1 (1973).

43. C. Elachi and P. Yeh, "Periodic Structures in Integrated Optics," *J. Appl. Phys.*, **44**, 3146 (1973).

44. S. T. Peng, H. L. Bertoni, and T. Tamir, "Analysis of Periodic Thin Film Structures with Rectangular Profiles," *Opt. Commun.*, **10**, 91 (1974).

45. T. G. Giallorenzi, "Acousto-Optical Deflection in Thin-Film Waveguides," *J. Appl. Phys.*, **4**, 242 (1973).

46. C. C. Ghizoni, J. M. Ballantyne, and C. L. Tang, "Theory of Optical Waveguide

Distributed Feedback Lasers: A Green's Function Approach," *IEEE J. Quantum Electron.*, **QE–13**, 843 (1977).

47. H. M. Stoll, "Distributed Bragg Deflector: A Multifunctional Integrated Optical Device," *Appl. Opt.*, **17**, 2562 (1978).

48. R. Normandin, V. C-Y. So, N. Rowell, and G. I. Stegeman, "Scattering of Guided Optical Beams by Surface Acoustic Waves in Thin Films," *J. Opt. Soc. Am.*, **69**, 1153 (1979).

49. V. C-Y. So, R. Normandin, and G. I. Stegeman, "Field Analysis of Harmonic Generation in Thin Film Integrated Optics," *J. Opt. Soc. Am.*, **69**, 1166 (1979).

50. J. E. Sipe and G. I. Stegeman, "Comparison of Normal Mode and Total Field Analysis Techniques in Planar Integrated Optics," *J. Opt. Soc. Am.*, **69**, 1676 (1979).

51. G. I. Stegeman, D. Sarid, J. J. Burke, and D. G. Hall, "Scattering of Guided Waves by Surface Periodic Gratings for Arbitrary Angles of Incidence: Perturbation Field Theory and Implications to Normal-Mode Analysis," *J. Opt. Soc. Am.*, **71**, 1497 (1981).

52. E. Bradley and D. G. Hall, "Out-of-Plane Scattering from Glass Waveguides: Comparison of Theory and Experiment," *Opt. Lett.*, **7**, 235 (1982).

53. L. A. Weller-Brophy and D. G. Hall, "Analysis of Waveguide Gratings: Application of Rouard's Method," *J. Opt. Soc. Am. A*, **2**, 863 (1985).

54. L. A. Weller-Brophy and D. G. Hall, "Analysis of Waveguide Gratings: A Comparison of the Results of Rouard's Method and Coupled-Mode Theory," *J. Opt. Soc. Am. A*, **4**, 60 (1987).

55. D. Marcuse, "Coupled-Mode Theory for Anisotropic Optical Waveguides," *Bell Syst. Tech. J.*, **54**, 985 (1975).

56. D. Marcuse, "Electro-Optic Coupling Between TE and TM Modes in Anisotropic Slabs," *IEEE J. Quantum Electron.*, **QE–11**, 759 (1977).

57. E. N. Glytsis, T. K. Gaylord, and M. G. Moharam, "Electric Field, Permittivity, and Strain Distributions Induced by Interdigitated Electrodes on Electro-Optic waveguides," *J. Lightwave Technol.*, **LT–5**, 668 (1987).

58. E. N. Glytsis and T. K. Gaylord, "Rigorous Three-Dimensional Coupled-Wave Diffraction Analysis of Single and Cascaded Anisotropic Gratings," *J. Opt. Soc. Am.*, **A4**, 2061 (1987).

59. A. Knoesen, "Guided Modes in Anisotropic Dielectric Planar Waveguides," Ph.D. Thesis, Georgia Institute of Technology, 1987.

60. A. Knoesen, T. K. Gaylord, and M. G. Moharam, "Hybrid Guided Modes in Uniaxial Dielectric Planar Waveguides," *J. Lightwave Technol.*, **LT–6**, xxx (1988) (accepted).

FIGURE CAPTIONS

1. (a) Three-dimensional geometry of the diffraction of guided-waves in uniaxial anisotropic slab waveguides by interdigitated-electrode induced phase gratings. (b) A top-view of the same geometry that shows the various diffraction directions of the ordinary and extraordinary components of an incident mode, for each diffracted order. In this figure only the 0- and +1-orders are shown.

2. The decomposition of a guided mode into four plane wave components. $O+$ and $O-$ are the two ordinary plane wave components while $E+$ and $E-$ are the two extraordinary plane wave components.

3. Decomposition of the guided mode diffraction problem into four grating diffraction subproblems.

4. Planar slices through wavevector surfaces for the case of the optic axis being perpendicular to the electrode surface. (a) zz_w plane intersection at $y_w = 0$, (b) xy plane intersection at $z = 0$, (c) xy plane intersection at $x_w = \pm k_{xw/O}$, corresponding to the ordinary waves $O+$ and $O-$ (TE modes), and (d) xy plane intersection at $x_w = \pm k_{xw/E}$, corresponding to the two extraordinary waves $E+$ and $E-$ (TM modes).

5. Top-view (xy plane) of the diffraction geometry in the case of the optic axis perpendicular to the electrode surface. The 0-order and the i-order forward-diffracted directions are shown. (a) TE incident mode ($O+$, $O-$ waves), and (b) TM incident mode ($E+$, $E-$ waves). The directions shown are valid for a negative birefringent material. In the case of positive birefringent material the relative ordering of the diffraction angles is reversed.

6. Planar slices through wavevector surfaces for the case of the optic axis being in the

electrode plane. (a) zz_w plane intersection at $y_w = 0$, (b) xy plane intersection at $z = 0$, (c) xy plane intersection at $x_w = \pm k_{xwfO}$, corresponding to the two ordinary plane wave components, and (d) xy plane intersection at $x_w = \pm k_{xwfE}$, corresponding to the two extraordinary plane wave components.

7. Top-view (xy plane) of the diffracted geometry in the case of the optic axis lying in the electrode plane. Only the 0-order and the i-order forward-diffracted waves are shown for (a) general incidence and optic axis orientation, and (b) for Bragg incidence and optic axis orientation restricted along the x or the y axis.

8. xy plane intersections of the wavevector surfaces at $x_w = \pm k_{xwfO}$, that correspond to the ordinary waves, and at $x_w = \pm k_{xwfE}$, that corresponds to the extraordinary waves. The Bragg condition is also satisfied. (a) Optic axis along the x axis, and (b) optic axis along the y axis.

9. The general relation of the complex coefficients f_{iO+}, f_{iO-}, f_{iE+}, and f_{iE-}, in the complex plane. Coefficients ratios with respect to f_{iO+} are shown.

10. xy plane intersections of the wavevector surfaces for the case of the optic axis being perpendicular to the electrode surface, and for a slanted electrode configuration. (a) A TE incident mode (ordinary waves), and (b) a TM incident mode (extraordinary waves).

11. xy plane intersections of the wavevector surfaces at $x_w = \pm k_{xwfO}$ (ordinary waves) and $x_w = \pm k_{xwfE}$ (extraordinary waves) for Bragg incidence and (a) optic axis orientation parallel to the grating vector, and (b) optic axis orientation perpendicular to the grating vector.

12. Top-view (xy plane) geometry of a Givens rotation device.[23]

13. The diffracted electric fields of the Givens rotation device as a function of the applied

electrode voltage. The dotted lines correspond to rigorously calculated results while the continuous lines correspond to a best cosine or sine fit. (a) 0-order forward-diffracted fields, and (b) +1-order (Bragg) forward-diffracted fields.

14. (a) The top-view of the herringbone multiplier. (b) The wavevector diagram (xy plane intersection) that corresponds to the herringbone multiplier. The incident wavevector, $\vec{k}_1$, the Bragg diffracted wavevectors, $\vec{\sigma}_1$ and $\vec{\sigma}_2$, and the grating vectors, $\vec{K}_1$ and $\vec{K}_2$ are shown.

15. The efficiency of the -2-order forward-diffracted mode, the predicted efficiency from the approximate formula $DE_{pr} = K_* V_1 V_2$, and the percentage error $(DE_{pr} - DE) \times 100/DE$, as functions of the applied voltages ($V = V_1 = V_2$).

16. Diffraction efficiencies of the $O+$, $O-$, $E+$, and $E-$ forward-diffracted waves as a function of the applied voltage for (a) the 0-order, and (b) the Bragg-order.

17. Diffracted phases of the $O+$, $O-$, $E+$, and $E-$ forward-diffracted waves as a function of the applied voltage for (a) the 0-order, and (b) the Bragg-order.

18. Diffraction efficiencies of the 0-order forward-diffracted mode (dashed line), and of the Bragg-order diffracted mode (continuous line) as a function of the applied voltage. In these plots, the computed solutions are given by the solid dots. The continuous and the dashed lines, calculated by cubic spline interpolation, have been provided for ease of interpretation.

19. The theoretical (continuous line) and the experimental (circles) mode diffraction efficiencies of the interdigitated-electrode correlator[18] as a function of the applied voltage.

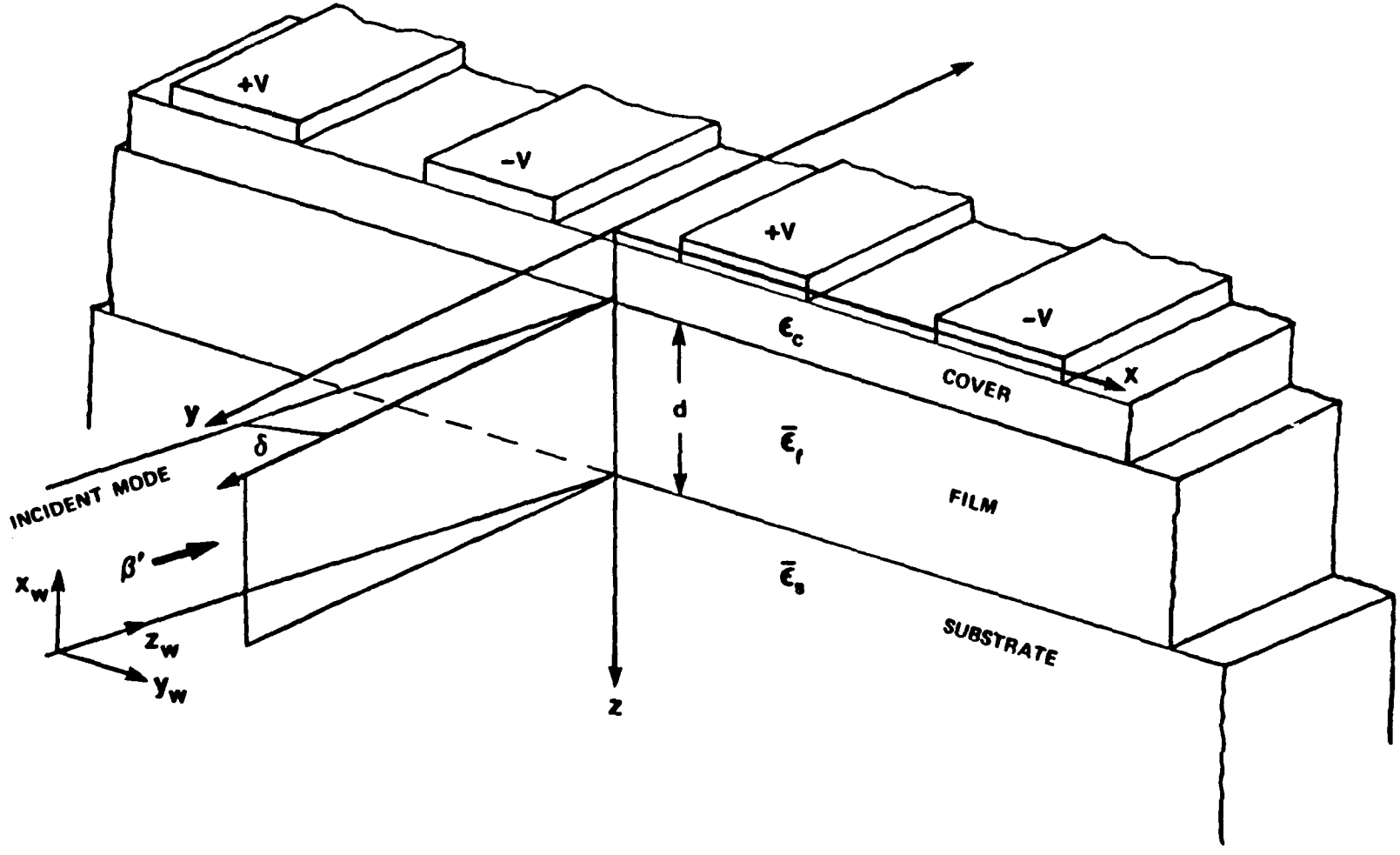
+V
-V
+V
-V
ϵ_c
COVER
x
y
d
δ
$\bar{\epsilon}_f$
FILM
INCIDENT MODE
β'
x_w
z_w
y_w
$\bar{\epsilon}_s$
SUBSTRATE
z

Fig.1a

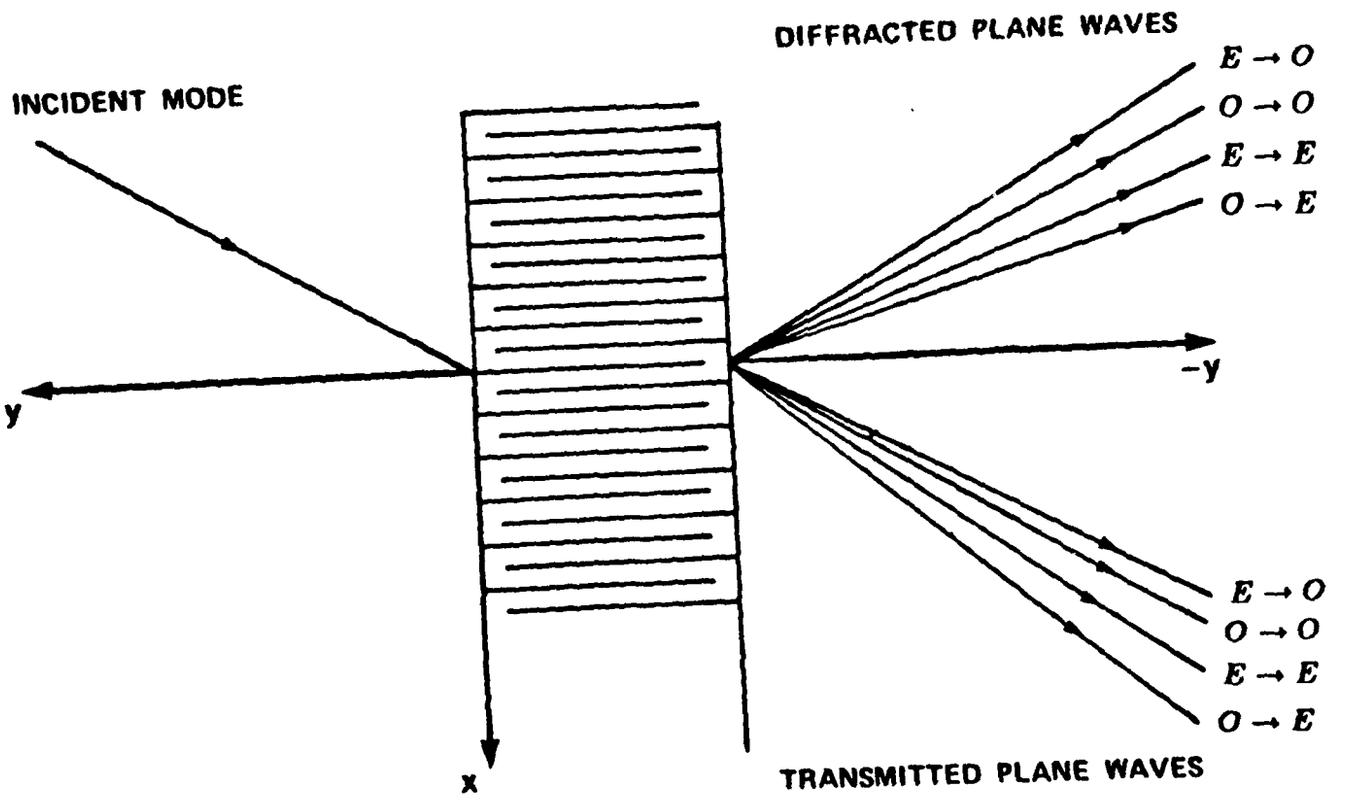
DIFFRACTED PLANE WAVES
INCIDENT MODE
E → O
O → O
E → E
O → E
-y
y
x
E → O
O → O
E → E
O → E
TRANSMITTED PLANE WAVES

Fig.1b

GUIDED MODE DECOMPOSITION

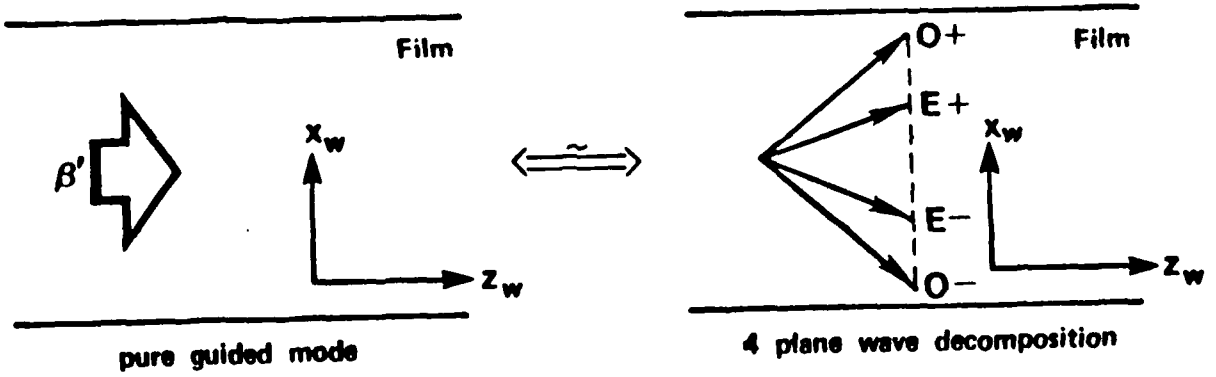

Fig. 2

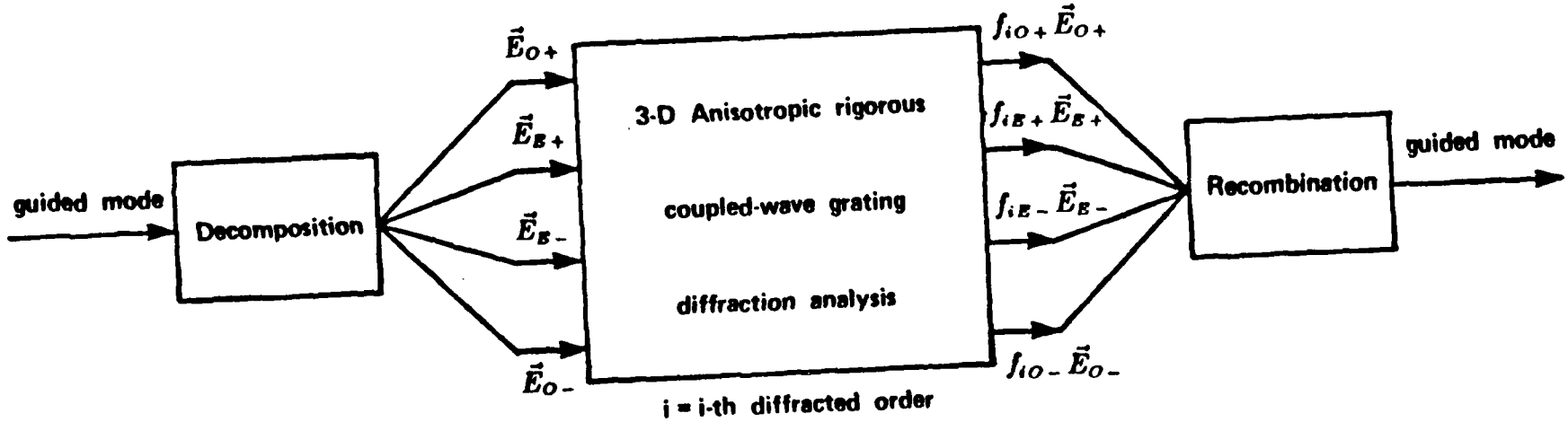

$$f_{iw} = \frac{\text{diffracted amplitude}}{\text{incident amplitude}} \qquad w = O+,\ O-,\ E+,\ E-$$

Fig. 3

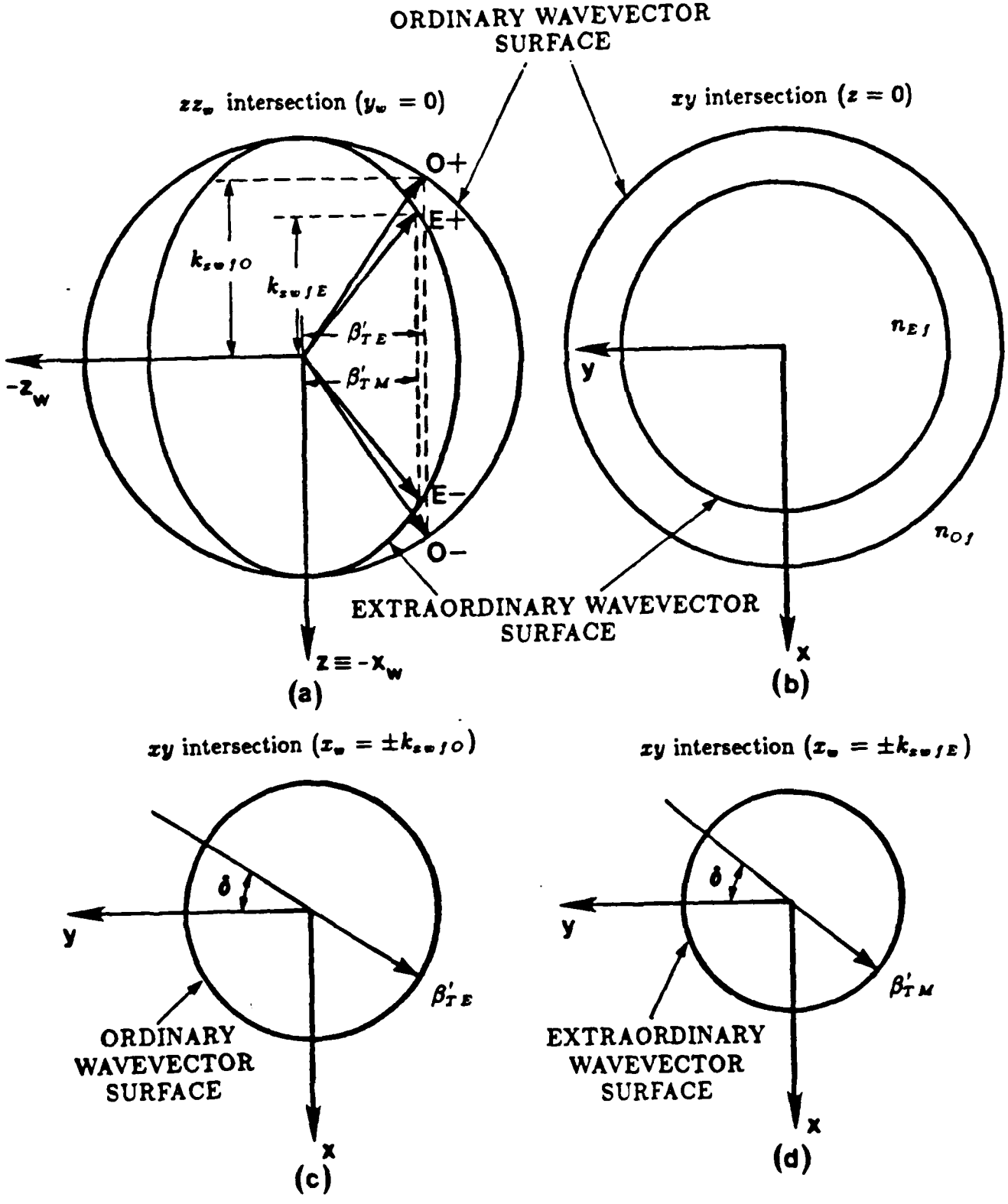
ORDINARY WAVEVECTOR SURFACE
zz_w intersection ($y_w = 0$)
xy intersection ($z = 0$)
O+
E+
k_{zwfO}
k_{zwfE}
β'_{TE}
β'_{TM}
$-z_w$
E−
O−
n_{Ef}
n_{Of}
y
EXTRAORDINARY WAVEVECTOR SURFACE
$z \equiv -x_w$
x
(a)
(b)
xy intersection ($x_w = \pm k_{zwfO}$)
xy intersection ($x_w = \pm k_{zwfE}$)
δ
y
β'_{TE}
ORDINARY WAVEVECTOR SURFACE
x
(c)
δ
y
β'_{TM}
EXTRAORDINARY WAVEVECTOR SURFACE
x
(d)

Fig. 4

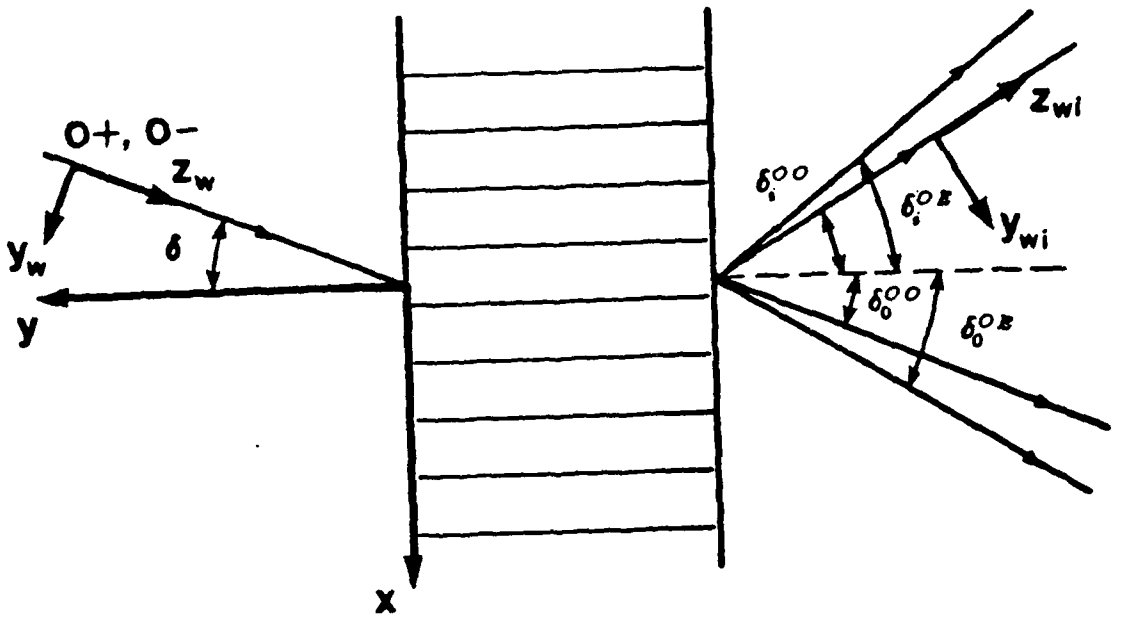
O+, O−
z_w
y_w
δ
y
x
z_{wi}
y_{wi}
δ_i^{OO}
δ_i^{OE}
δ_0^{OO}
δ_0^{OE}

(a)

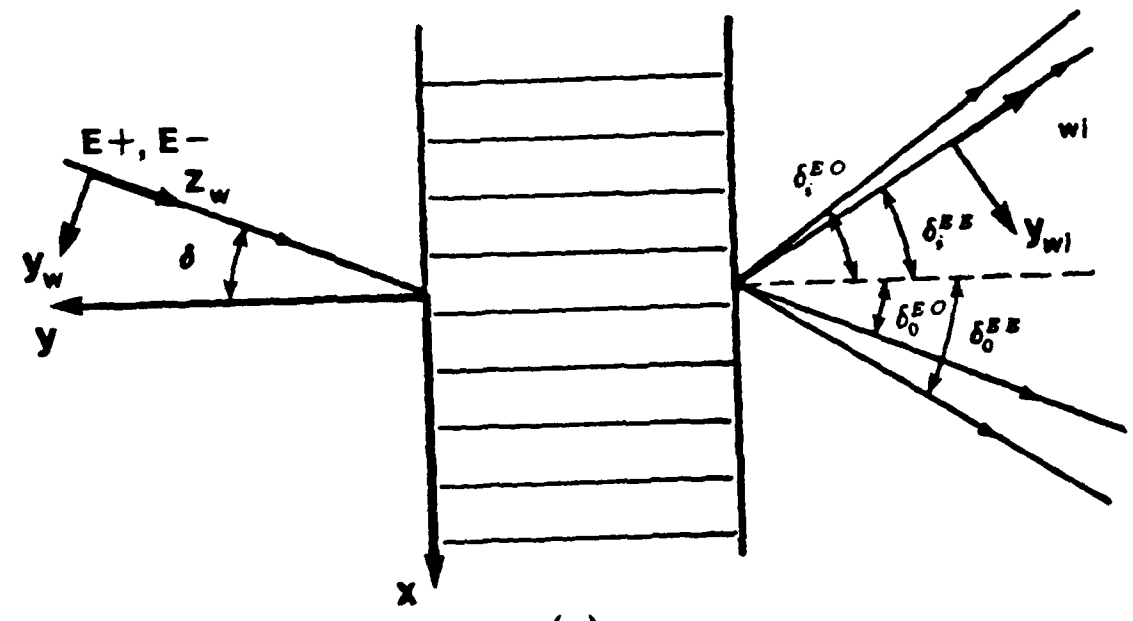
E+, E−
z_w
y_w
δ
y
x
wi
y_{wi}
δ_i^{EO}
δ_i^{EE}
δ_0^{EO}
δ_0^{EE}

(b)

Fig. 5

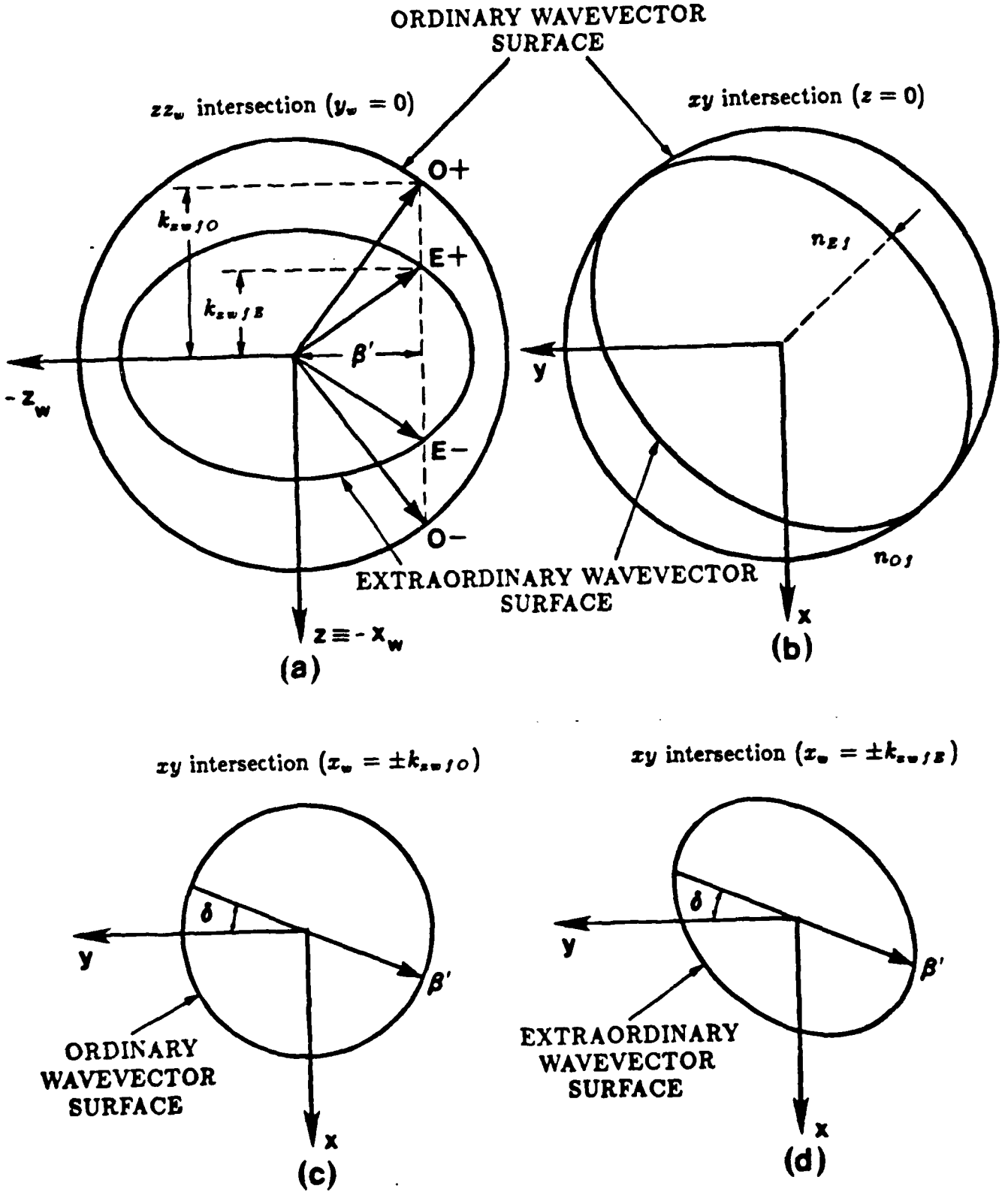
ORDINARY WAVEVECTOR SURFACE
zz_w intersection ($y_w = 0$)
xy intersection ($z = 0$)
O+
E+
E−
O−
k_{zw} jO
k_{zw} jE
β′
$-z_w$
$z \equiv -x_w$
(a)
n_{Ej}
n_{Oj}
y
x
(b)
EXTRAORDINARY WAVEVECTOR SURFACE
xy intersection ($x_w = \pm k_{zw}$ jO)
xy intersection ($x_w = \pm k_{zw}$ jE)
δ
y
β′
x
ORDINARY WAVEVECTOR SURFACE
(c)
EXTRAORDINARY WAVEVECTOR SURFACE
(d)

Fig. 6

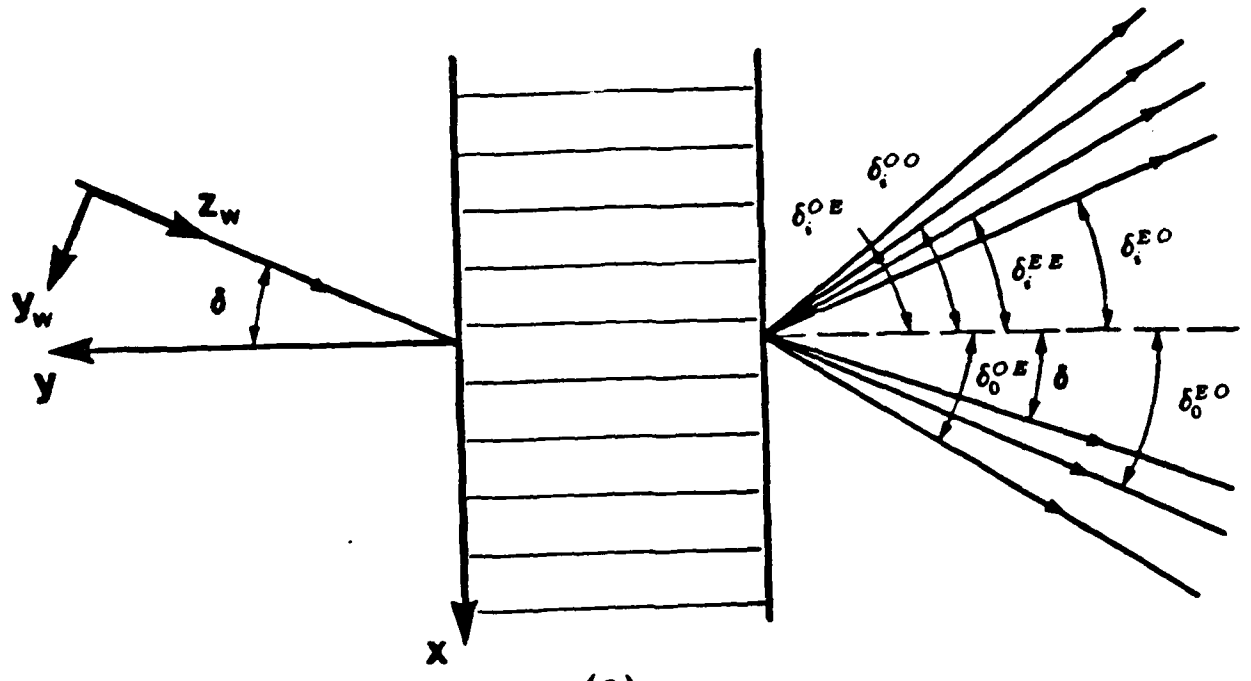
z_w
y_w
δ
y
x
δ_i^{OO}
δ_i^{OE}
δ_i^{EE}
δ_i^{EO}
δ_0^{OE}
δ
δ_0^{EO}

(a)

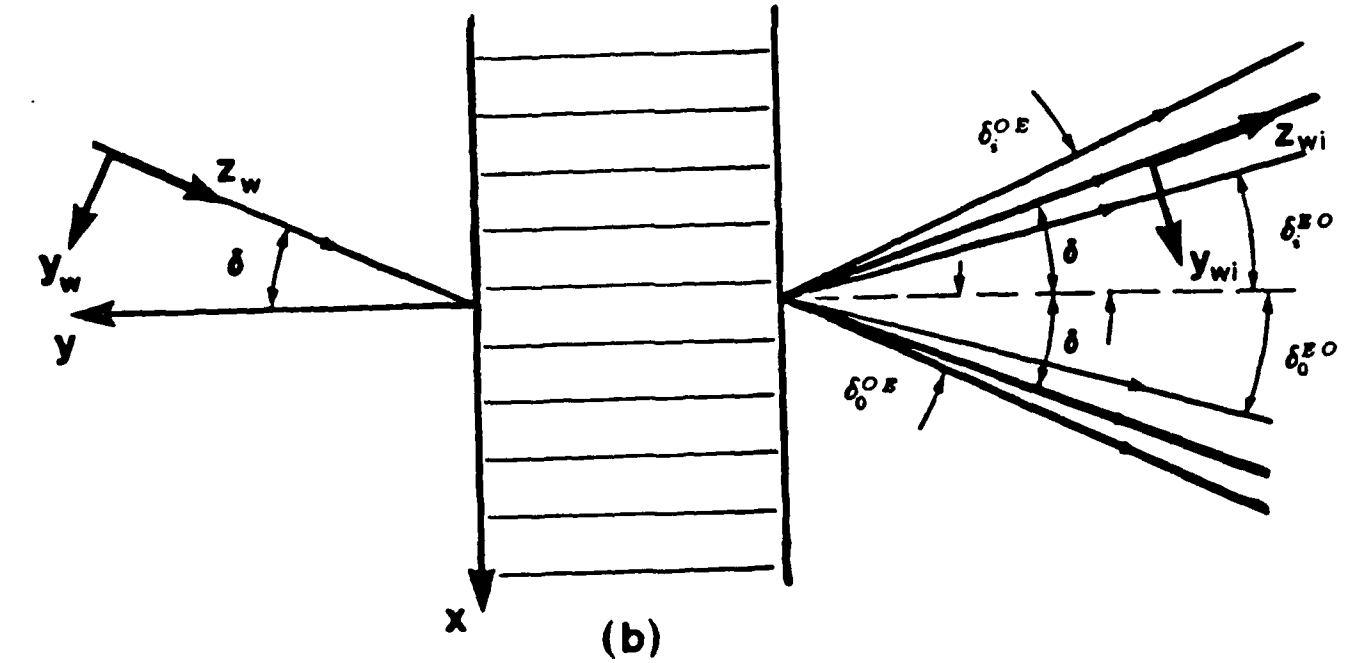
z_w
y_w
δ
y
x
δ_i^{OE}
z_{wi}
δ_i^{EO}
δ
y_{wi}
δ
δ_0^{EO}
δ_0^{OE}

(b)

Fig. 7

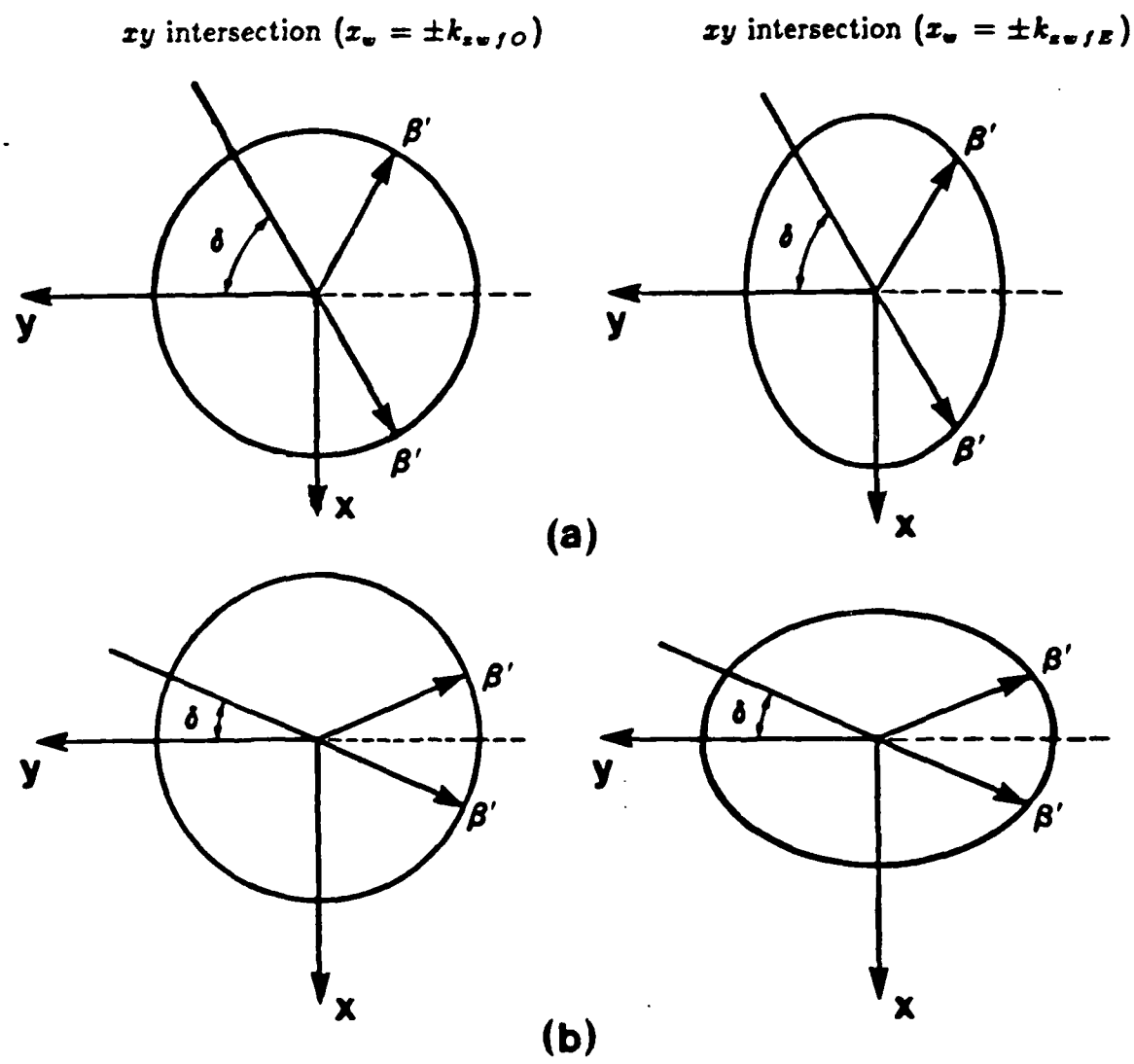
xy intersection ($x_w = \pm k_{xw/O}$)
xy intersection ($x_w = \pm k_{xw/E}$)
β′
δ
y
x
(a)
(b)

Fig. 8

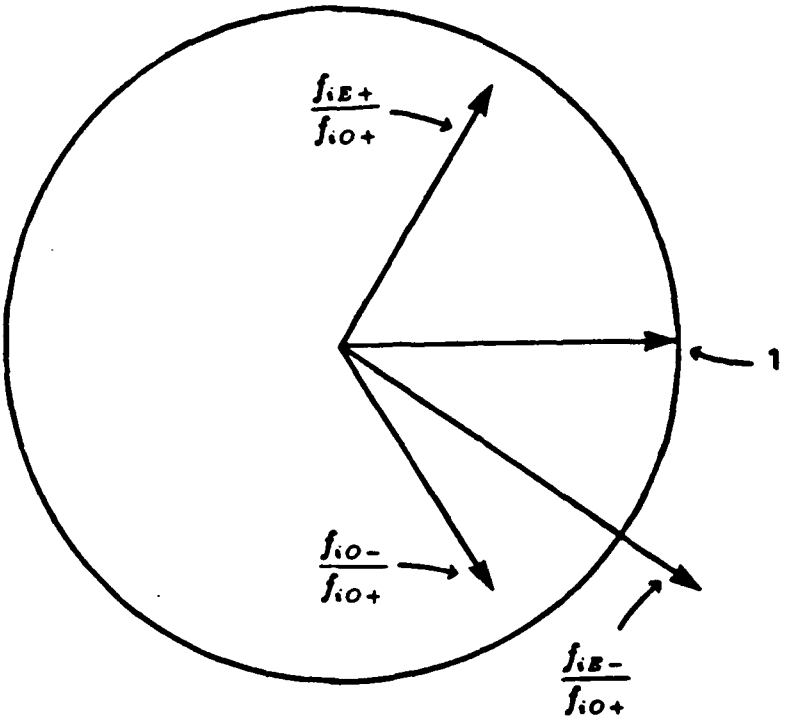

Fig. 9

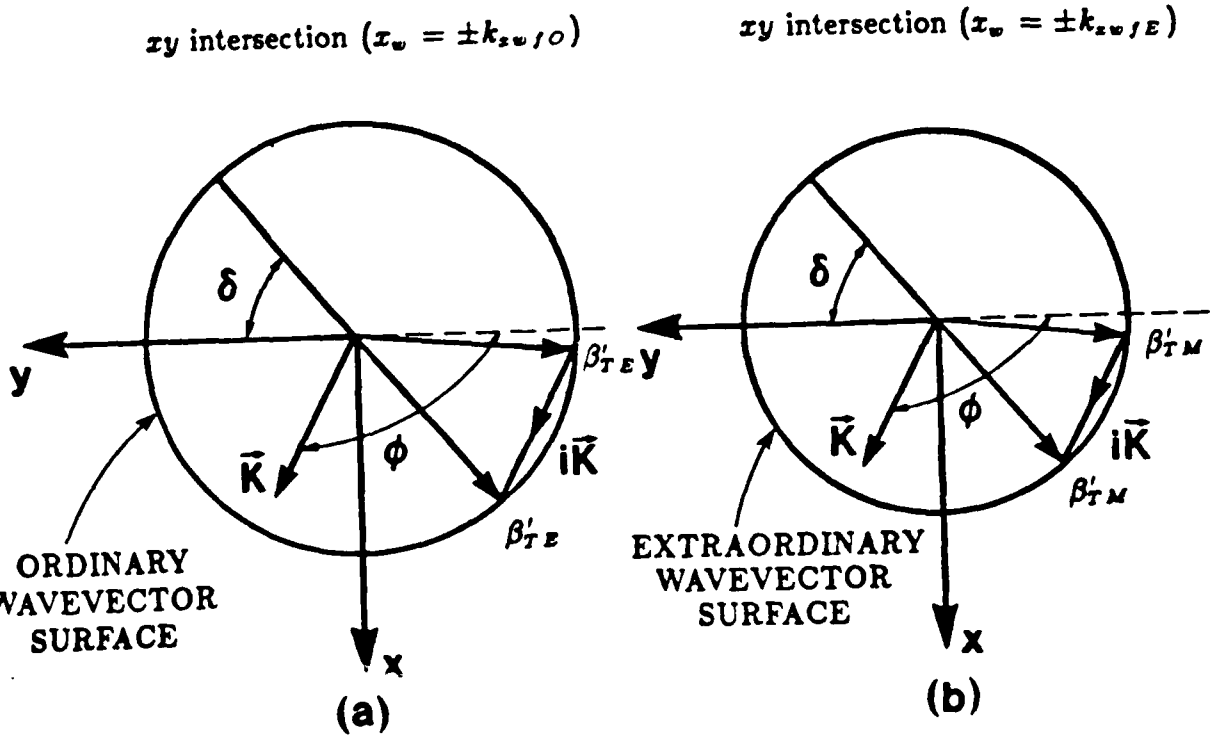
xy intersection ($x_w = \pm k_{xw/O}$)
xy intersection ($x_w = \pm k_{xw/E}$)
δ
y
β'_{TE}
$\vec{K}$
ϕ
$i\vec{K}$
β'_{TE}
ORDINARY WAVEVECTOR SURFACE
x
(a)
δ
y
β'_{TM}
$\vec{K}$
ϕ
$i\vec{K}$
β'_{TM}
EXTRAORDINARY WAVEVECTOR SURFACE
x
(b)

Fig.10

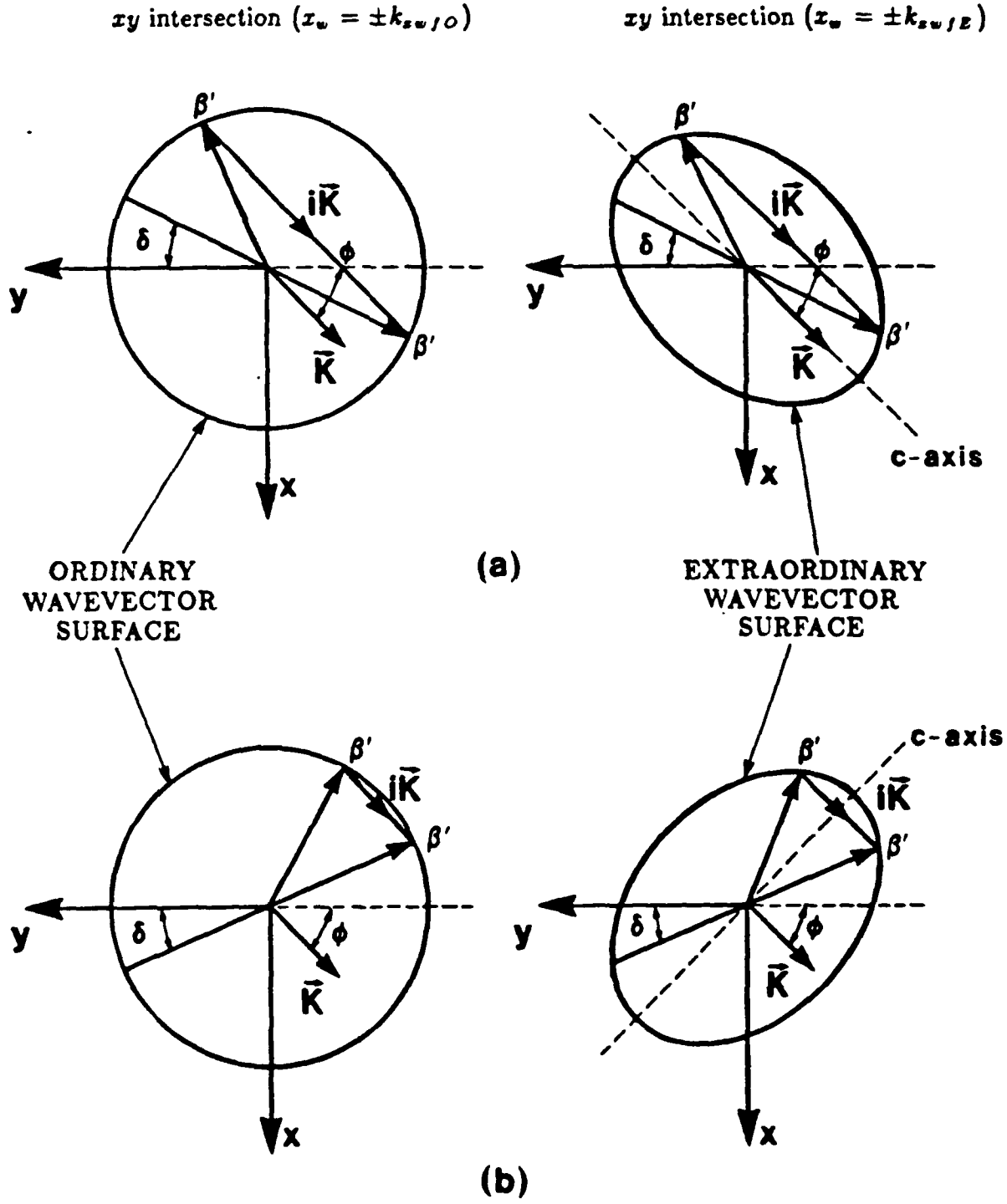
xy intersection ($x_w = \pm k_{sw/O}$)
xy intersection ($x_w = \pm k_{sw/E}$)
β′
iK⃗
δ
ϕ
K⃗
y
x
c-axis
ORDINARY WAVEVECTOR SURFACE
EXTRAORDINARY WAVEVECTOR SURFACE
(a)
(b)

Fig. 11

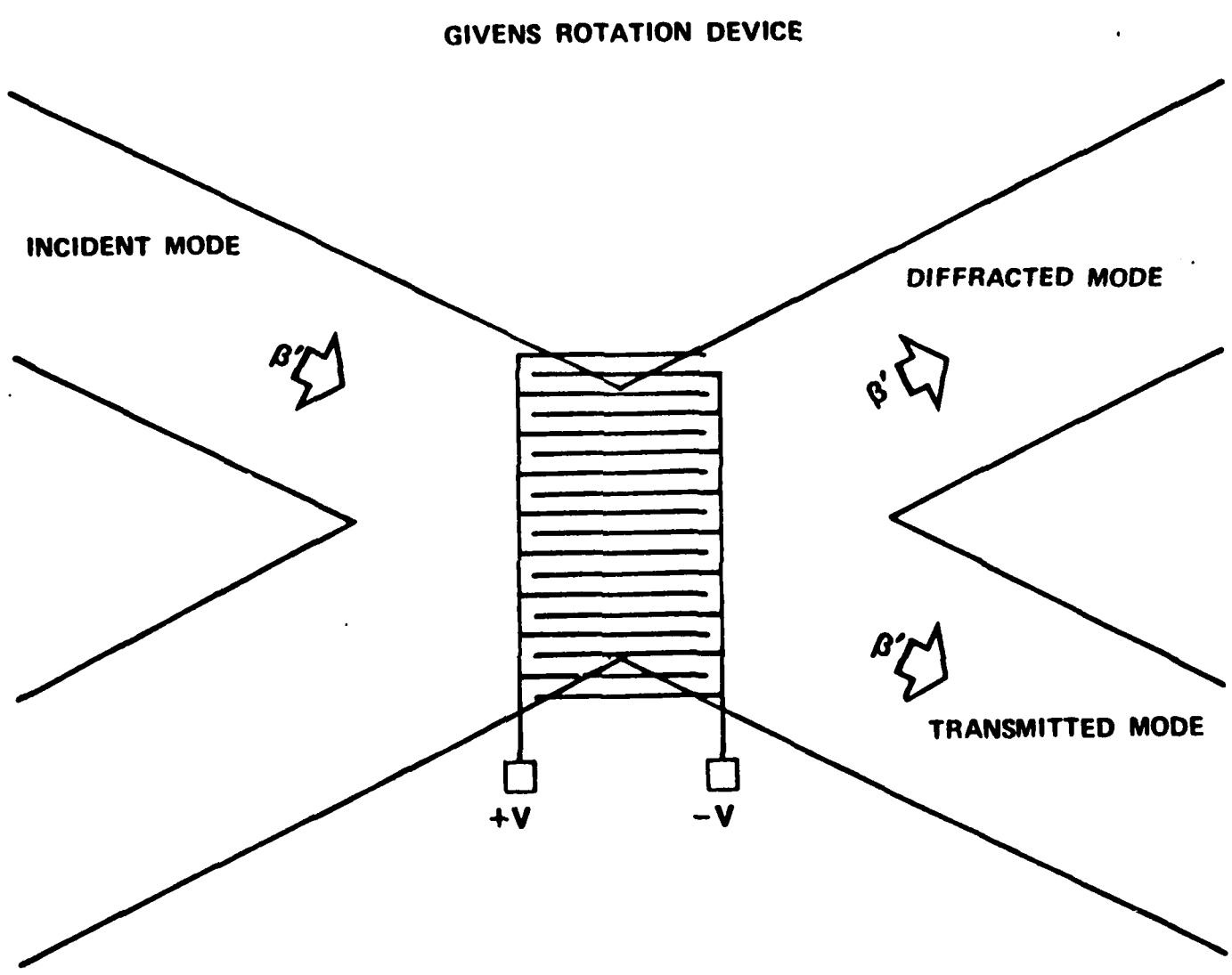
GIVENS ROTATION DEVICE
INCIDENT MODE
DIFFRACTED MODE
β'
β'
β'
TRANSMITTED MODE
+V
-V

Fig.12

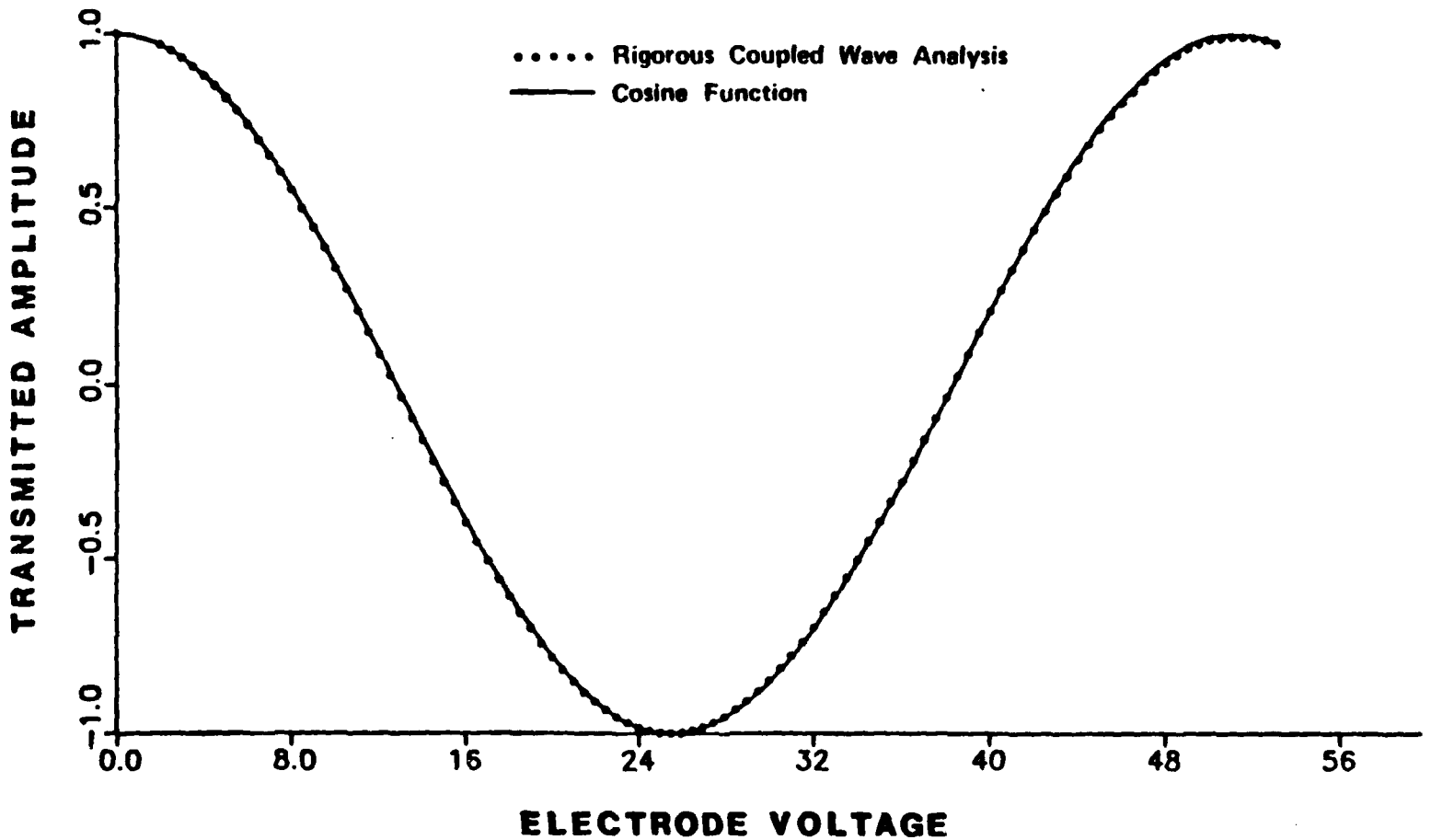
Rigorous Coupled Wave Analysis
Cosine Function
TRANSMITTED AMPLITUDE
1.0
0.5
0.0
-0.5
-1.0
0.0
8.0
16
24
32
40
48
56
ELECTRODE VOLTAGE

Fig.13a

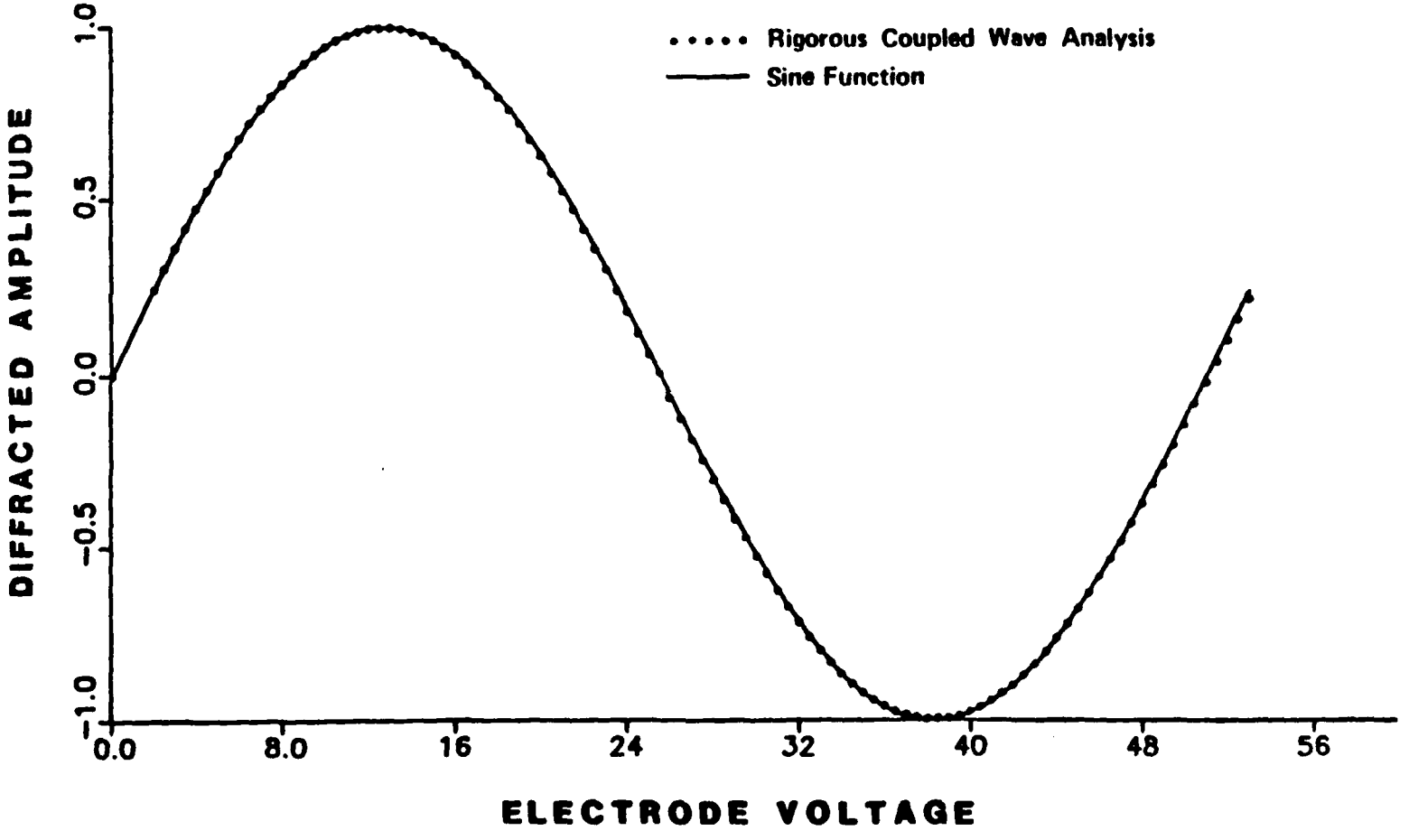
Rigorous Coupled Wave Analysis
Sine Function
DIFFRACTED AMPLITUDE
1.0
0.5
0.0
-0.5
-1.0
0.0
8.0
16
24
32
40
48
56
ELECTRODE VOLTAGE

Fig.13b

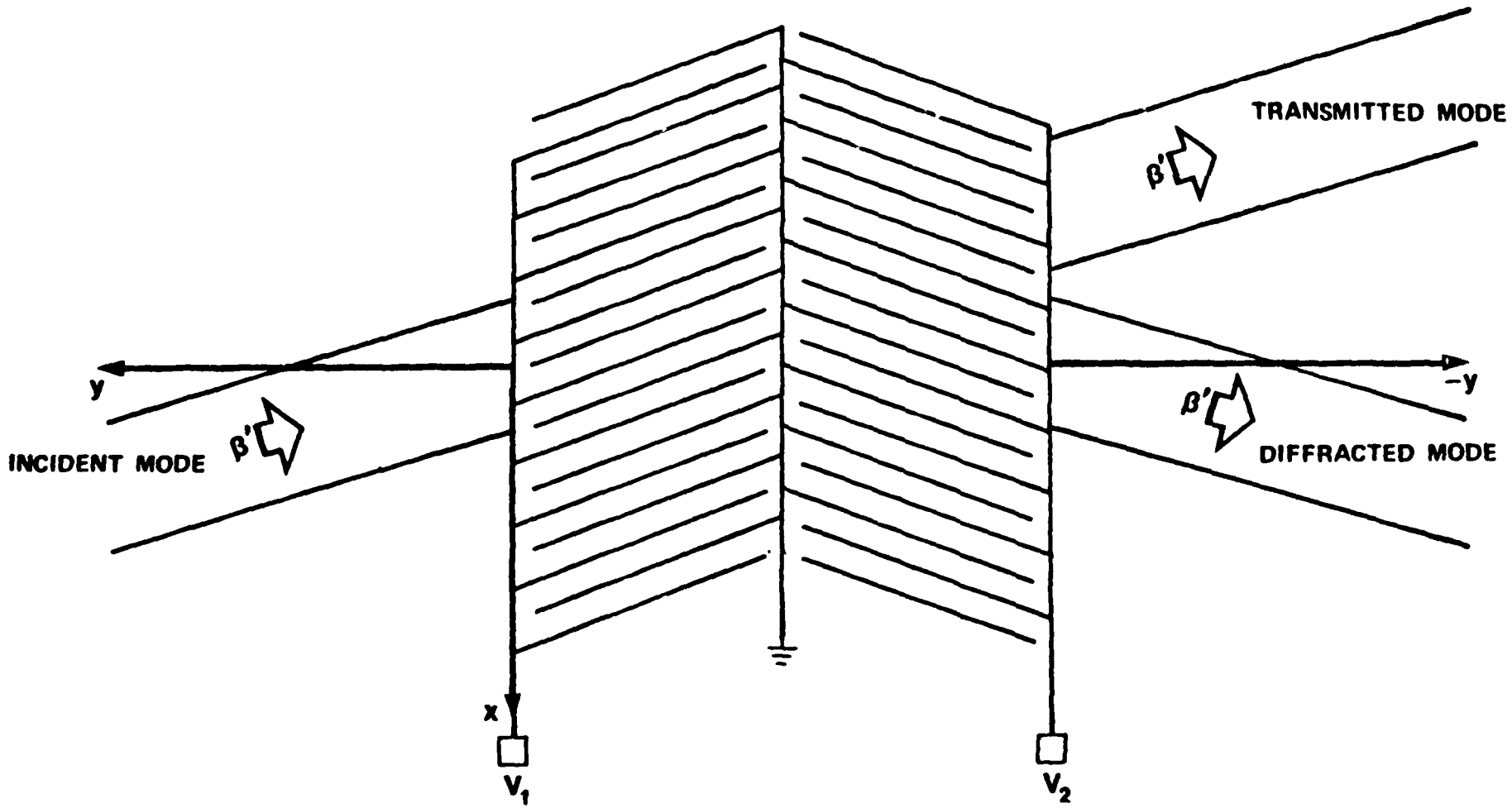
TRANSMITTED MODE
β'
y
-y
INCIDENT MODE
β'
β'
DIFFRACTED MODE
x
V1
V2

Fig.14a

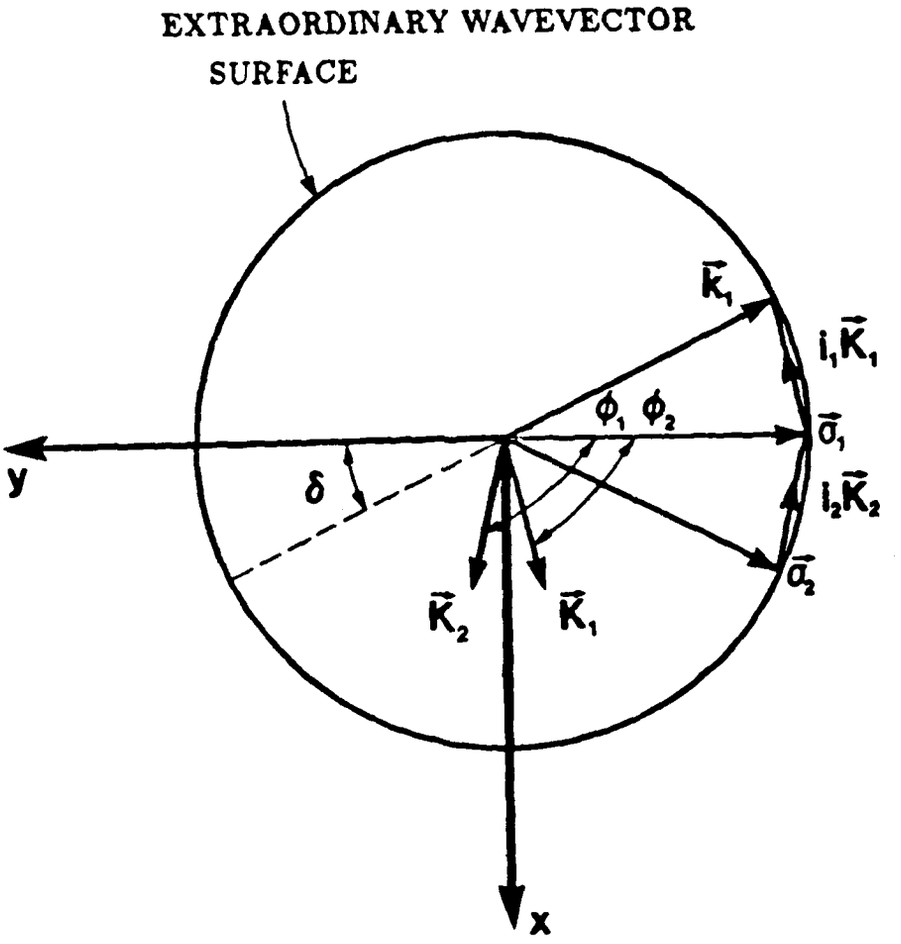
EXTRAORDINARY WAVEVECTOR
SURFACE
$\vec{K}_1$
$i_1\vec{K}_1$
ϕ_1 ϕ_2
$\vec{\sigma}_1$
y
δ
$i_2\vec{K}_2$
$\vec{\sigma}_2$
$\vec{K}_2$
$\vec{K}_1$
x

Fig.14b

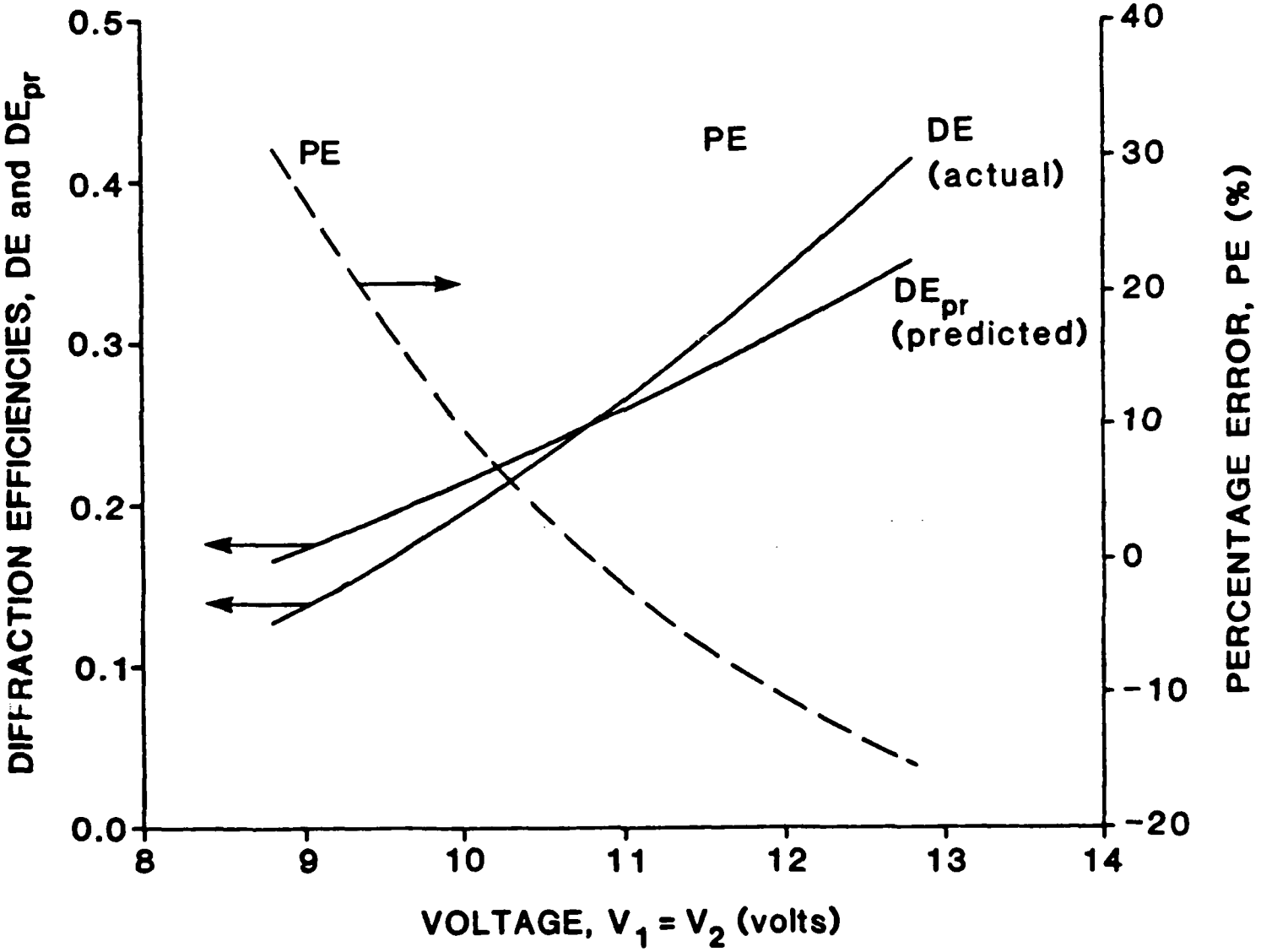
0.5
0.4
0.3
0.2
0.1
0.0
40
30
20
10
0
-10
-20
8
9
10
11
12
13
14
PE
PE
DE
(actual)
DE$_{pr}$
(predicted)
DIFFRACTION EFFICIENCIES, DE and DE$_{pr}$
PERCENTAGE ERROR, PE (%)
VOLTAGE, $V_1 = V_2$ (volts)

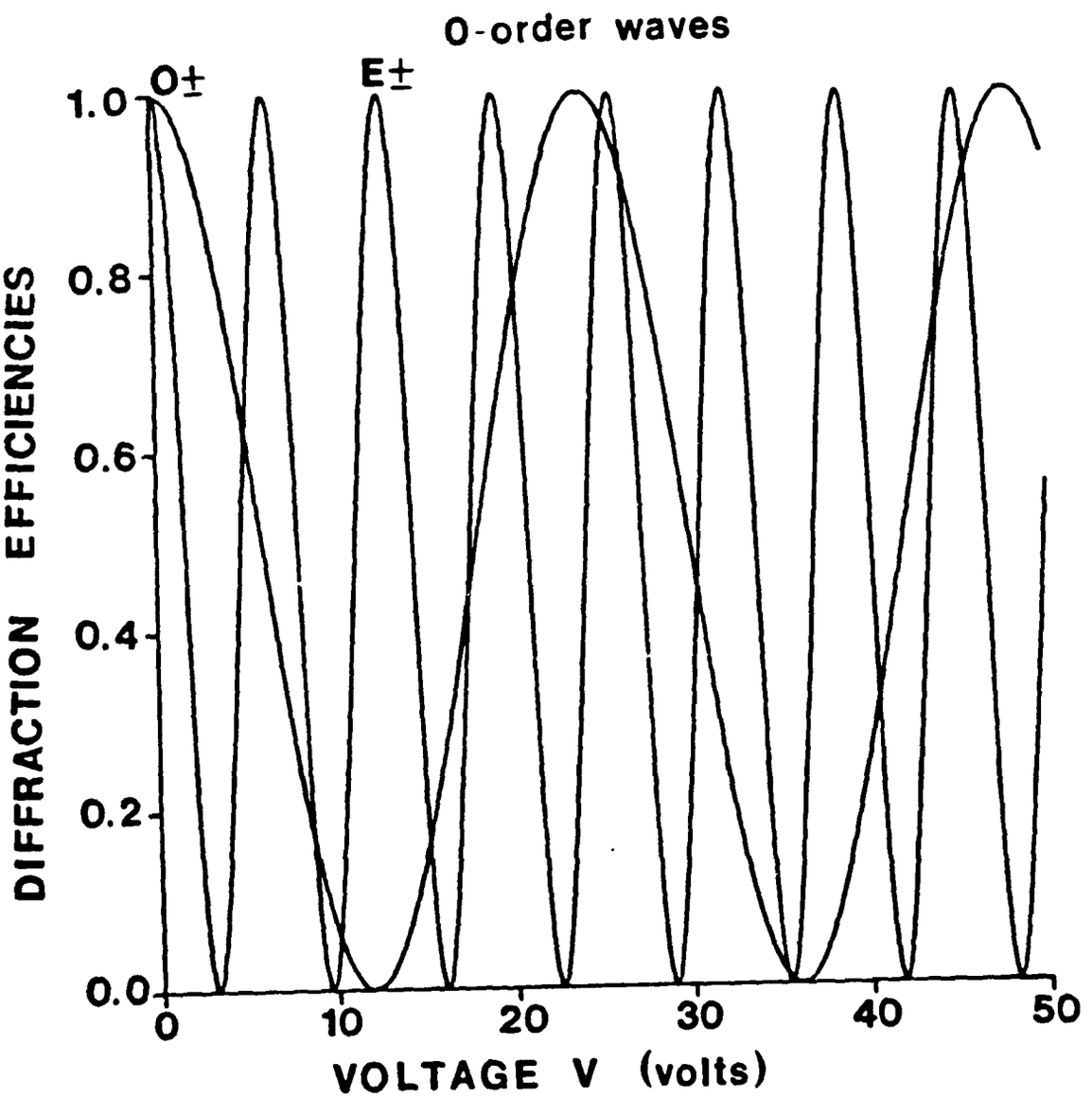
0-order waves
O±
E±
1.0
0.8
0.6
0.4
0.2
0.0
DIFFRACTION EFFICIENCIES
0
10
20
30
40
50
VOLTAGE V (volts)

Fig.16a

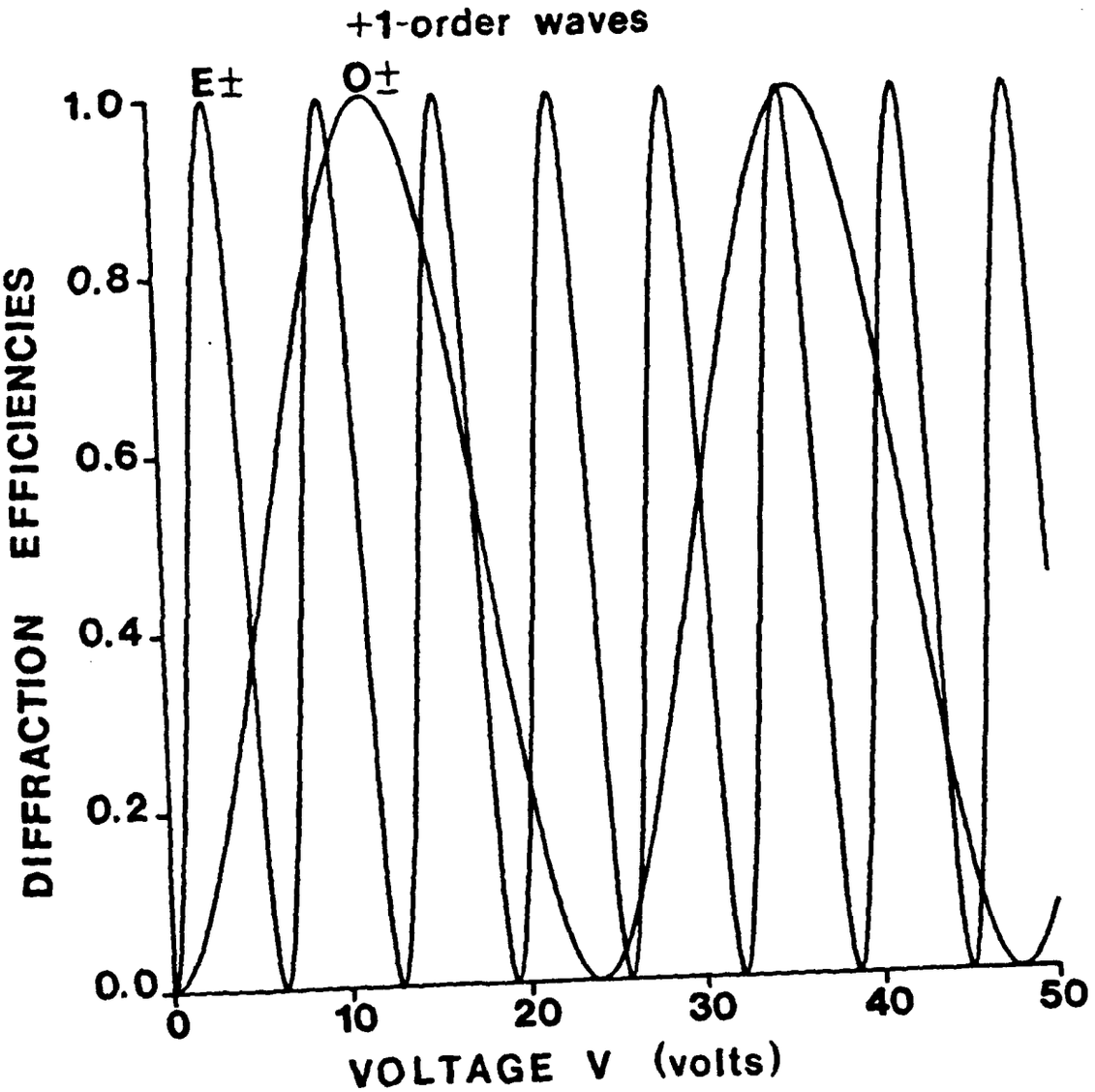
+1-order waves
E±
O±
1.0
0.8
0.6
0.4
0.2
0.0
DIFFRACTION EFFICIENCIES
0
10
20
30
40
50
VOLTAGE V (volts)

Fig.16b

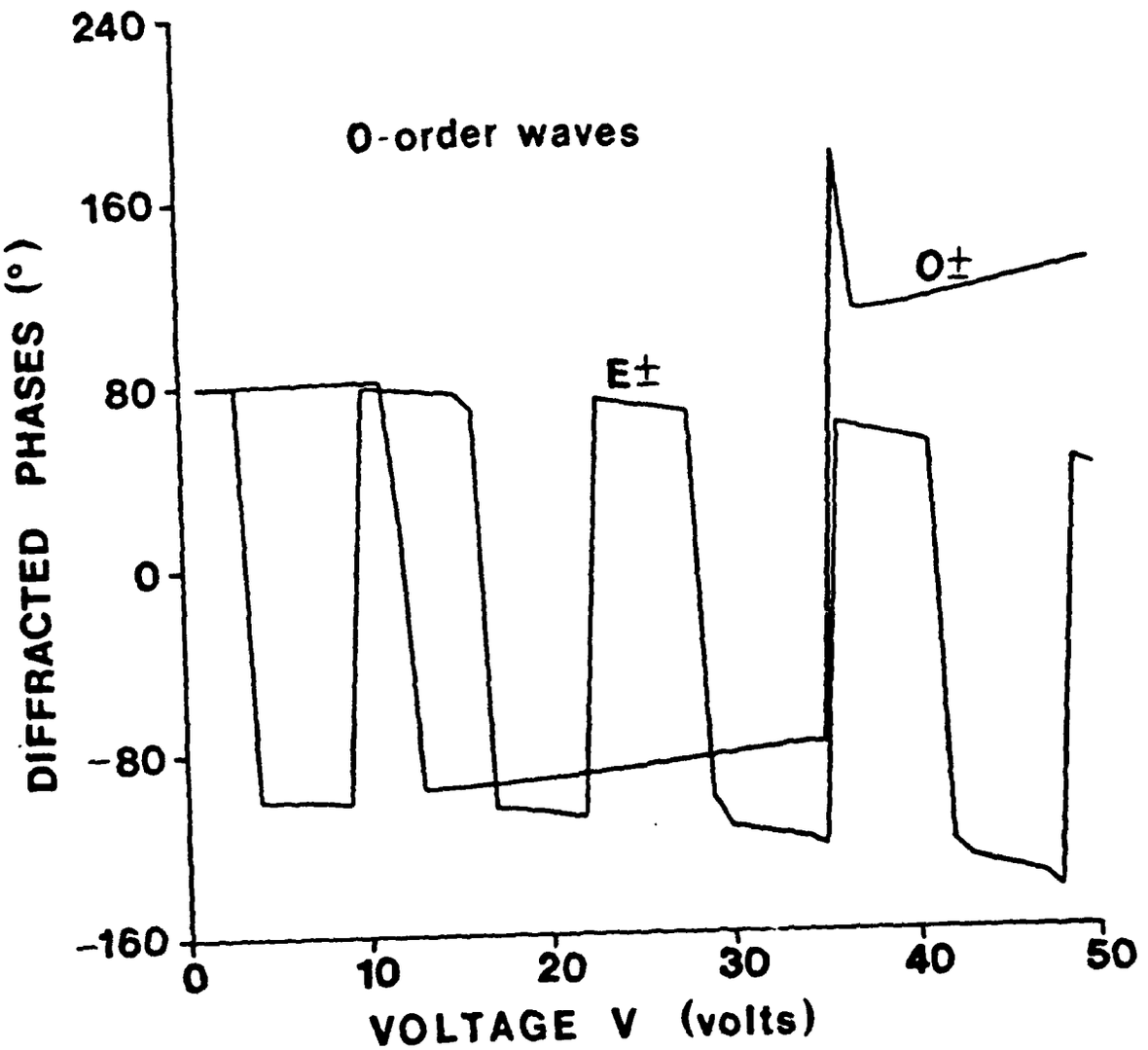
0-order waves
O±
E±
240
160
80
0
-80
-160
DIFFRACTED PHASES (°)
0
10
20
30
40
50
VOLTAGE V (volts)

Fig.17a

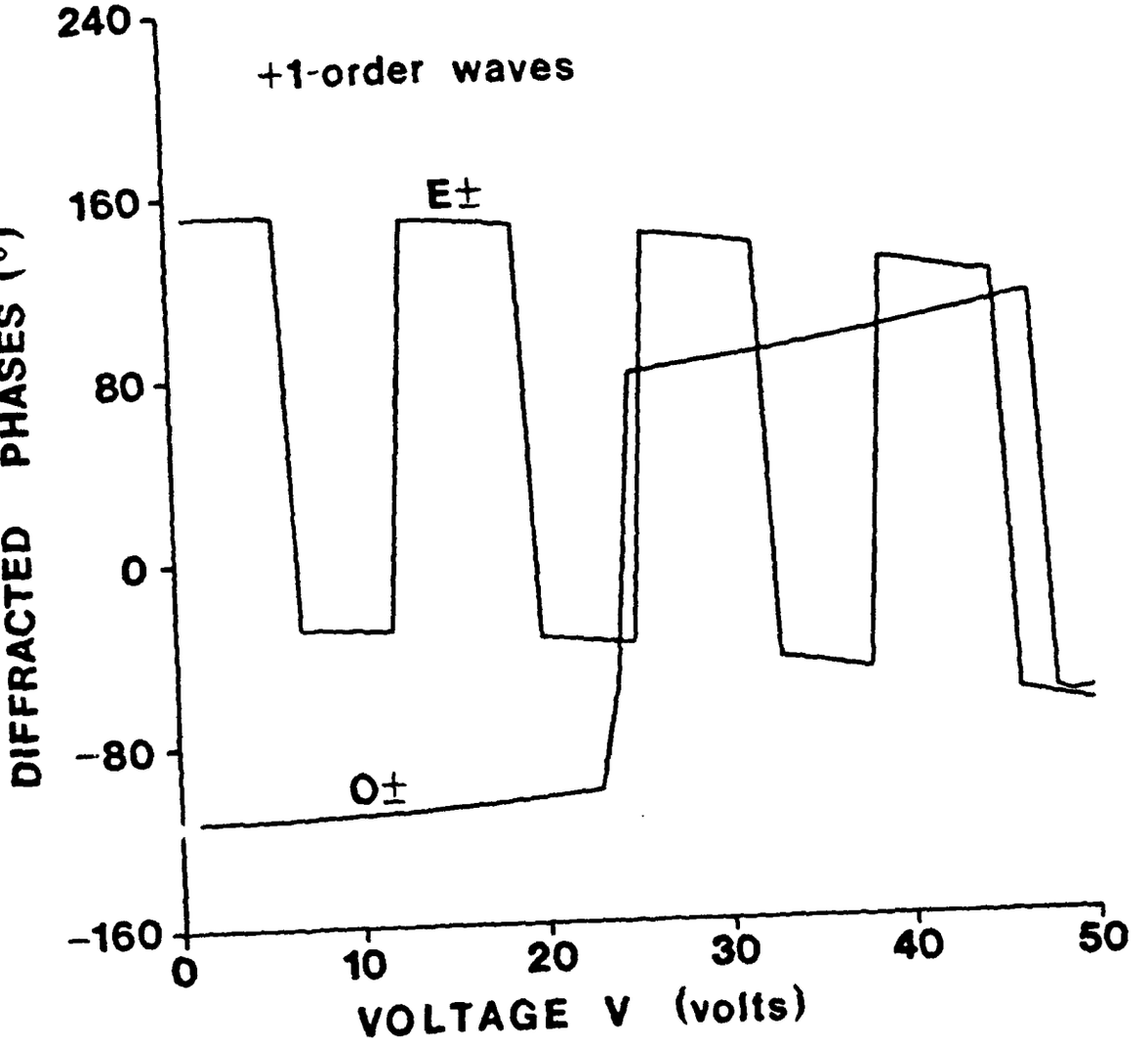
240
160
80
0
-80
-160
+1-order waves
E±
O±
DIFFRACTED PHASES (°)
0
10
20
30
40
50
VOLTAGE V (volts)

Fig.17b

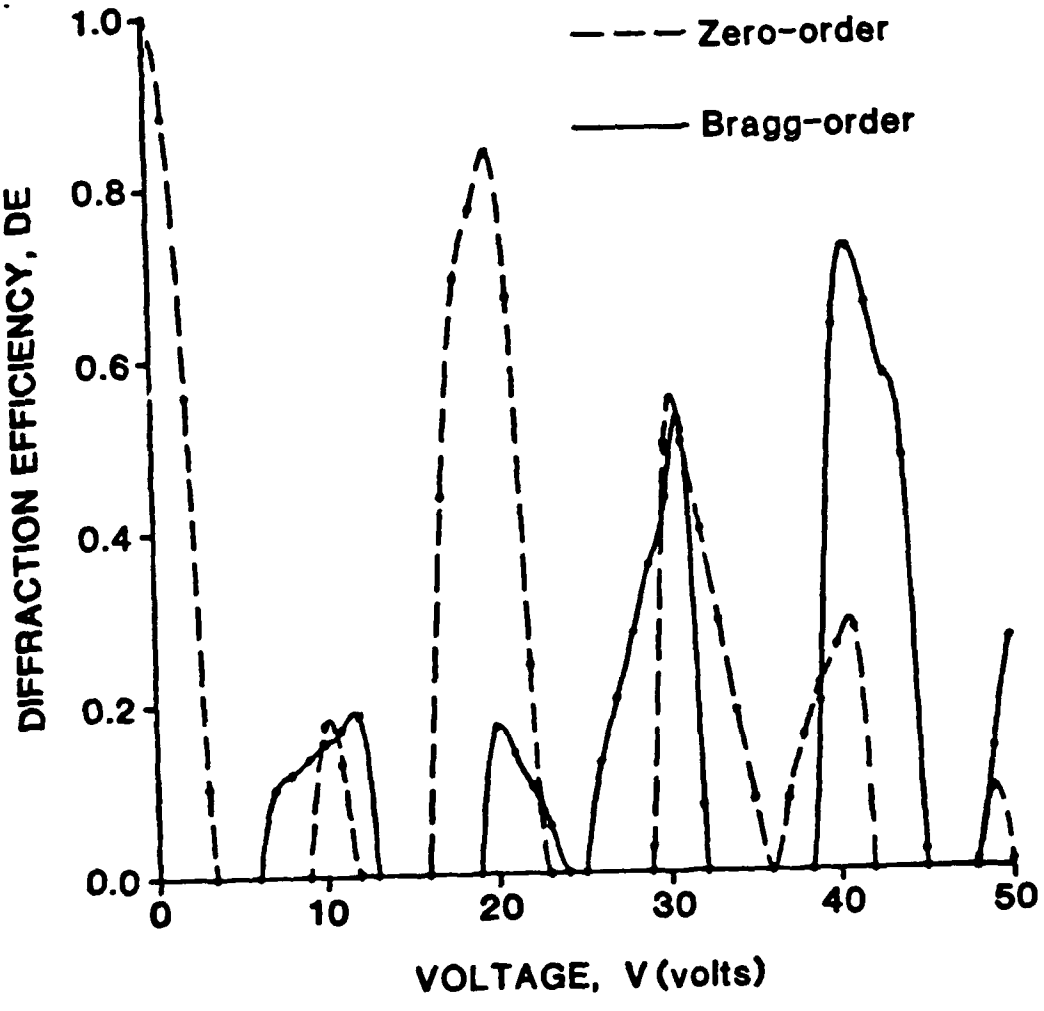
Zero-order
Bragg-order
DIFFRACTION EFFICIENCY, DE
1.0
0.8
0.6
0.4
0.2
0.0
0
10
20
30
40
50
VOLTAGE, V (volts)

Fig.18

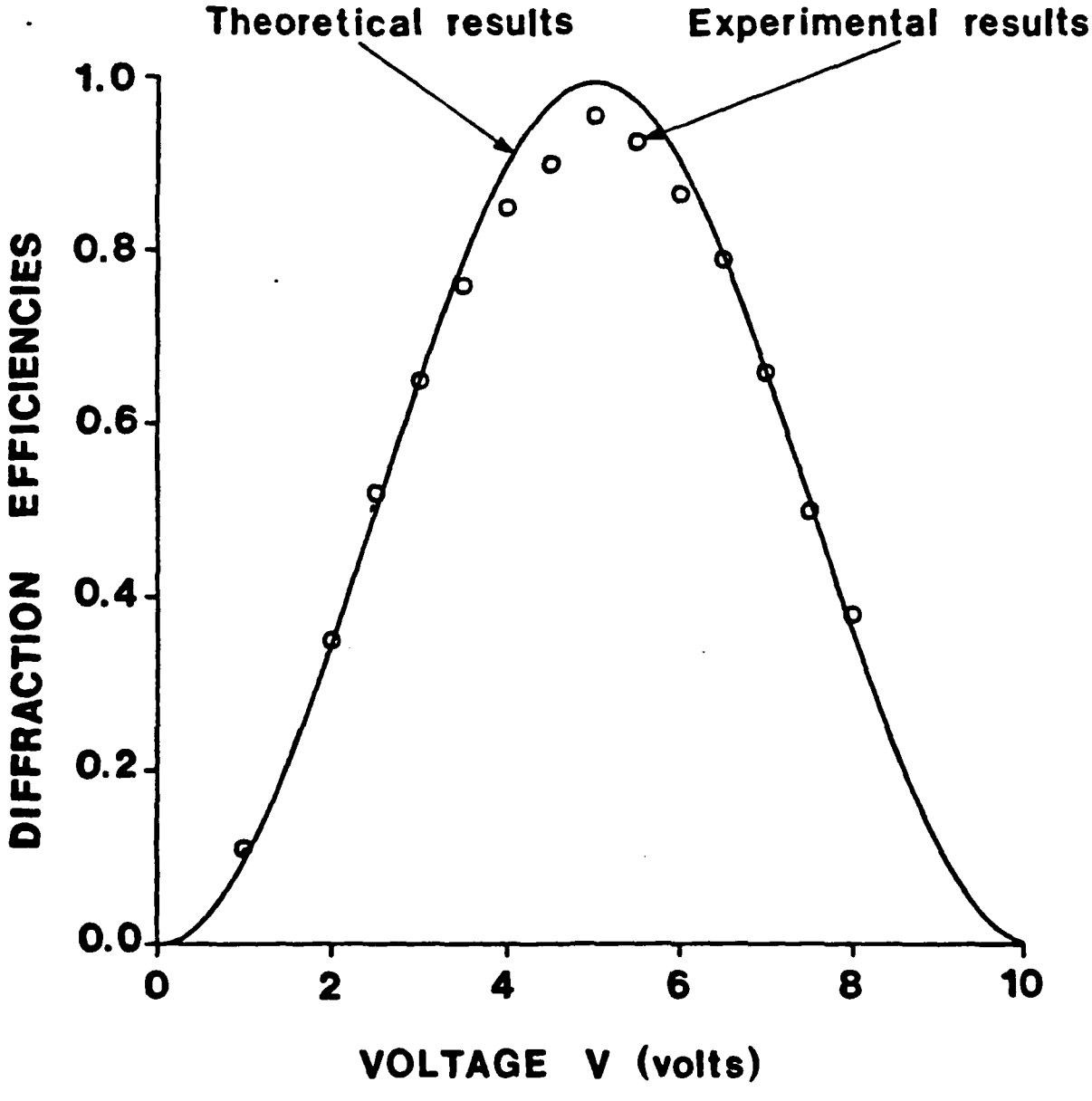
Theoretical results
Experimental results
DIFFRACTION EFFICIENCIES
1.0
0.8
0.6
0.4
0.2
0.0
0
2
4
6
8
10
VOLTAGE V (volts)